ELSEVIER

Marine Geology 209 (2004) 147–172

MARINE GEOLOGY
INTERNATIONAL JOURNAL OF MARINE GEOLOGY, GEOCHEMISTRY AND GEOPHYSICS

www.elsevier.com/locate/margeo

Seabed characterization on the New Jersey middle and outer shelf: correlatability and spatial variability of seafloor sediment properties

John A. Goff[a,b,*], Barbara J. Kraft[c], Larry A. Mayer[c], Steven G. Schock[d], Christopher K. Sommerfield[e], Hilary C. Olson[a,b], Sean P.S. Gulick[a,b], Sylvia Nordfjord[a,b]

[a] *Institute for Geophysics, University of Texas at Austin, 4412 Spicewood Springs Road, Building 600, Austin, TX 78759, USA*
[b] *John A. and Katherine G. Jackson School of Geosciences, University of Texas at Austin, Austin, TX 78712, USA*
[c] *Center for Coastal and Ocean Mapping, Chase Ocean Engineering Lab, University of New Hampshire, Durham, NH 03824, USA*
[d] *Department of Ocean Engineering, Florida Atlantic University, Boca Raton, FL 33431, USA*
[e] *College of Marine Studies, University of Delaware, Lewes, DE 19958, USA*

Received 4 September 2003; received in revised form 28 May 2004; accepted 28 May 2004

Abstract

Nearly 100 collocated grab samples and in situ 65 kHz acoustic measurements were collected on the New Jersey middle and outer shelf within an area that had previously been mapped with multibeam backscatter and bathymetry data, and more recently with chirp seismic reflection profiling. Eighteen short cores were also collected and probed for resistivity-based porosity measurements. The combined data set provides a basis for empirically exploring the relationship among the remotely sensed data, such as backscatter and reflection coefficients, and directly measured seabed properties such as grain size distribution, velocity, attenuation and porosity. We also investigate the spatial variability of these properties through semi-variogram analysis to facilitate acoustic modeling of natural environmental variability.

Grain size distributions on the New Jersey shelf are commonly multi-modal, leading us to separately characterize coarse % (>4 mm), fine % (<63 μm) and mean sand grain size to quantify the distribution. We find that the backscatter is dominated by the coarse component (expressed as weight %), typically shell hash and occasionally terrigenous gravel. In sediment types where coarse material is not significant, backscatter correlates with velocity and fine weight %. Mean sand grain size and fine % are partially correlated with each other, and combined represent the primary control on velocity. The fine %, rather than mean grain size as a whole, appears to be the primary control on attenuation, although coarse % may increase attenuation marginally through scattering. Vertical-incidence seismic reflection coefficients, carefully culled of unreliable values, exhibit a strong correlation with the in situ velocity measurements, suggesting that such data may prove more reliable than backscatter at deriving sediment physical properties from remote sensing data. The velocity and mean sand grain size semi-variograms can be fitted with a von Kármán statistical model with horizontal scale ~12.6 km, which provides a basis for generating synthetic realizations.

* Corresponding author. Institute for Geophysics, University of Texas at Austin, 4412 Spicewood Springs Road, Building 600, Austin, TX 78759, USA. Tel.: +1-512-471-0476; fax: +1-512-471-0999.
E-mail address: goff@ig.utexas.edu (J.A. Goff).

0025-3227/$ - see front matter
doi:10.1016/j.margeo.2004.05.030

The backscatter and coarse % semi-variograms exhibit two horizontal scales: one ~8 km and the other too small to quantify with available data.

Keywords: backscatter; grain size; velocity; attenuation; porosity; impedance

1. Introduction

Detailed swath bathymetry, sidescan, seismic and sediment data collected on the middle and outer New Jersey continental shelf seafloor (Fig. 1) reveal a complex amalgamation of bottom types and geomorphic features (Goff et al., 1999, 2000; Duncan et al., 2000; Duncan and Goff, 2001; Fig. 2). Moribund, winnowed and coarse grained sand ridges coexist with eroded swales of muddy sands; alternating bands of shelly muddy sands and well sorted medium sands form a ribboned mosaic over much of the sidescan map; gravel patches exist in several places, some where buried stream beds have been eroded to their base; and stiff clays on the outer shelf have preserved iceberg scours from the early Holocene. Data collection in this area has been extensive, owing in large part to efforts funded by the Office of Naval Research (ONR), including: (1) the STRATAFORM program (Nittrouer, 1999), which sought to understand the preservation of sedimentary strata in the upper 100 m; (2) the Geoclutter program (Austin et al., 2001), which is endeavoring to understand target-like acoustic returns from geologic heterogeneity, such as buried river channels; and (3) the Defense Research Initiative on Uncertainty in the Natural Environment, which seeks to understand the effect of oceanographic and seabed variability on detection uncertainty. To the

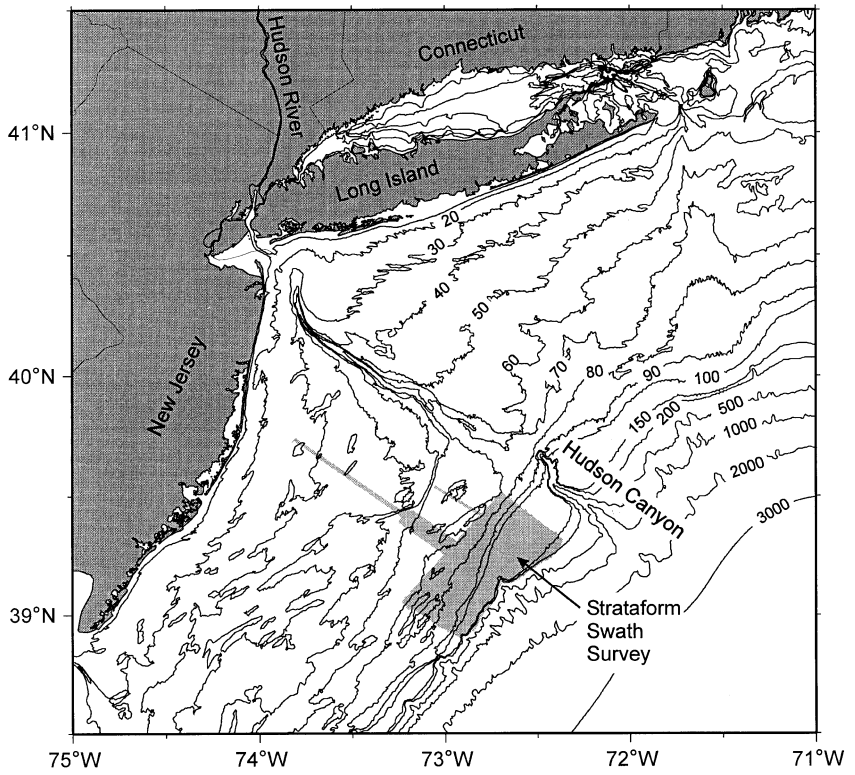

Fig. 1. Location map indicating location of the 1996 STRATAFORM swath map survey. Contours in meters.

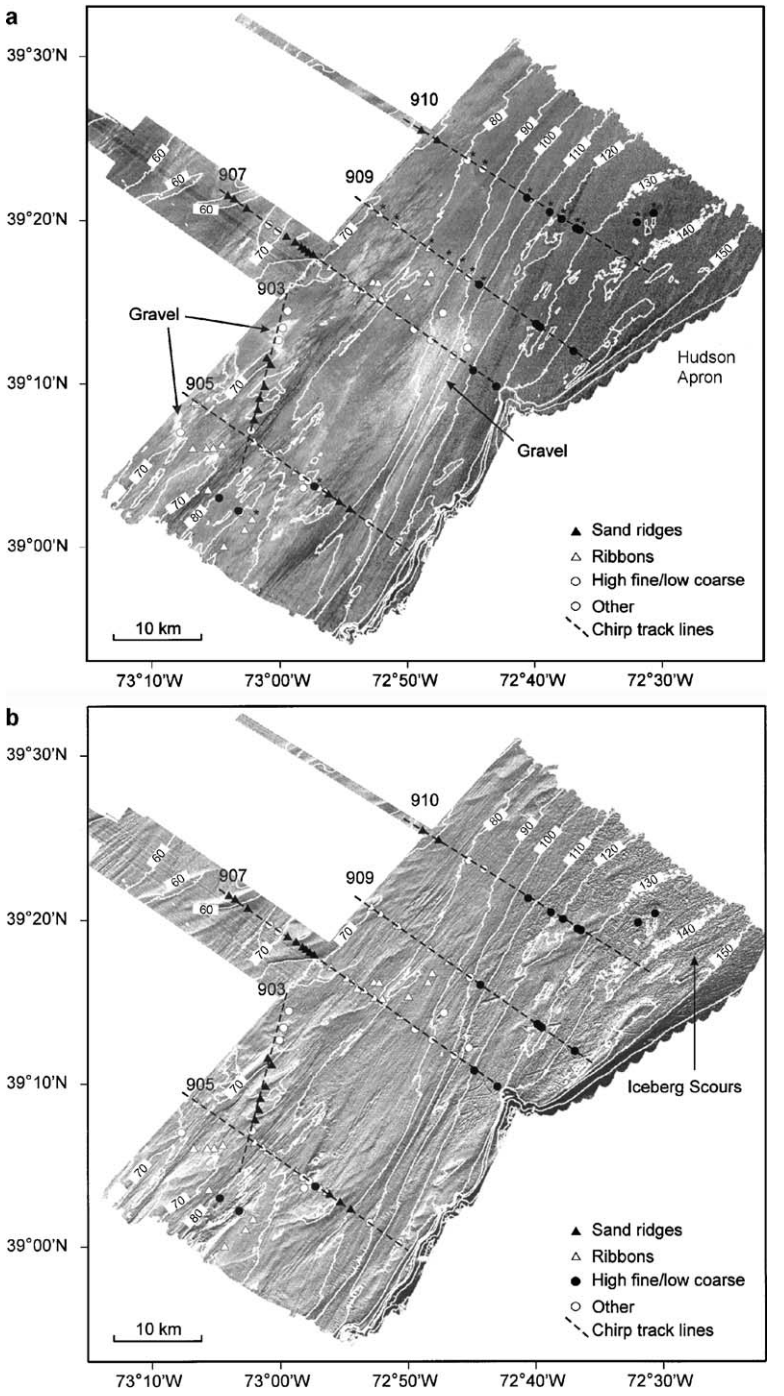

Fig. 2. (a) Sidescan and (b) swath bathymetry from the 1996 STRATAFORM swath map survey. Lighter shades in (a) indicate higher backscatter intensity. Bathymetry in (b) is artificially illuminated from the North. Contours are in meters. Symbols indicate station locations for grabs samples and ISSAP data. Stations at which short cores were also taken are indicated by asterisks. Heavy dashed lines indicate track lines (identified by numbers) of CHIRP seismic data used for reflection amplitude analysis. See text for explanation of sediment types.

Navy's acoustic interests in particular, the seabed is a critical interface, modulating reverberation and regulating the transfer of acoustic energy between ocean and sediment. Acoustic modeling in the shelfal domain requires accurate knowledge of the sediment/water interface, i.e., seafloor geomorphology, bulk physical properties (velocity, density, porosity, and attenuation), grain size distribution, and the spatial variability of each.

Because sampling involves extensive effort, seabed characterization over broad areas requires a combination of direct measurements and inference derived from remote sensing (e.g., swath mapping and seismic reflection surveying). Direct measurements should, in theory, provide ground truth for the remote sensing data, which can then be used to extrapolate our seabed characterization derived at the measurement sites. In practice, however, ground truthing remote sensing data can be complicated by the myriad factors. Sidescan backscatter, for example, is influenced by bathymetric slope, grain size roughness, bedform roughness, bulk properties and near-surface volumetric heterogeneities (e.g., Urick, 1983; Jackson et al., 1986). Because of the low bathymetric slopes on the New Jersey shelf (typically $\ll 1°$), the backscatter response (Fig. 2a) is dominated by sedimentary properties. However, careful ground truthing is required to make sense of it.

In this paper, we present empirical evidence on the correlatability of acoustic and physical properties of seafloor sediment on New Jersey mid- and outer shelf. The large range of sediment characteristics within the study area makes it a useful natural laboratory for this purpose. This setting is also likely analogous to a number of other siliciclastic shelf environments. Our primary motivation is to enable usage of the acoustic data as a proxy for physical properties of seafloor sediments, both for detailed geologic investigation and for acoustic modeling of our region of interest. Our primary data include: (1) acoustic backscatter (Goff et al., 1999; Fig. 2a); (2) vertical-incident reflection coefficients derived from chirp seismic reflection data (Austin et al., 2001); (3) grain size distribution derived from nearly 100 grab samples, (4) in situ velocity and attenuation measurements (Mayer et al., 2002; Kraft et al., 2002) collected coincident with grab samples, and (5) resistivity-based porosity estimates gathered from 18 short cores, which were collected primarily in finer-grained sediments. In unconsolidated sediments, porosity can be converted to density with simple assumptions regarding grain and pore water densities.

Spatial variability of sedimentary properties is another important concern for acoustic interaction with the seabed. In most acoustic detection scenarios, knowledge about seafloor physical properties will be severely limited. Unaccounted variability in the seabed will lead to uncertainty in acoustic detection variables. A quantitative understanding of seabed variability would provide two products: (1) a measure of acoustic detection uncertainty via input to acoustic models; and (2) a basis for cost–benefit analysis for seabed survey and sample work. Here, we investigate spatial variability of acoustic and physical properties of sediments on the New Jersey mid- and outer shelf through semi-variogram analysis.

2. Theoretical expectations

2.1. Backscatter

Theoretical expectations for the dependence of acoustic backscatter on sediment physical properties can be derived from Jackson et al.'s (1986) reformulation of Kuo's expression (Kuo, 1964) for backscattering cross section, σ_s, as a function of grazing angle θ:

$$\sigma_s(\theta) = 4k_a^4 \sin^4\theta F(\theta, v, \rho_{BW}) W(2k_a \cos\theta, 0), \qquad (1)$$

where k_a is the acoustic wavenumber, v is the ratio of acoustic velocity in sediments to that of water and ρ_{BW} is the ratio of bulk sediment density to water density. The bathymetric roughness spectrum, W, is specified at the "Bragg wavenumber" $2k_a\cos\theta$, which dominates the backscatter return. Thus, the scattering function can be very sensitive to the presence of roughness features that are on the order of an acoustic wavelength. The function F defines the dependence of scattering on bulk properties:

$$F(\theta, v, \rho) = \frac{\left[(\rho_{BW}-1)^2\cos^2\theta + \rho_{BW}^2 - v^{-2}\right]^2}{\left[\rho_{BW}\sin\theta + (v^{-2} - \cos^2\theta)^{1/2}\right]^4}, \quad \theta > \theta_{critical}. \qquad (2)$$

Jackson et al. (1986) computed a suite of solutions to Eq. (1) for values considered typical for sediment types ranging from silty clay to coarse sand. Given the sediment types exhibited on the New Jersey shelf, which mostly range from clayey sands to coarse sands, we might expect ~6 dB variation in backscatter strength due to variations in bulk properties of velocity and density, with higher backscatter values correlated to higher velocity and density.

Jackson et al. (1986) also presented a theoretical relationship for volumetric backscatter (their eq. (41)), which depends inversely on acoustic attenuation. Volumetric contributions are expected to be a minor component of the total backscatter for the primarily sandy sediments in the New Jersey shelf study area.

Ripples can also contribute to seabed roughness. On the outer New Jersey shelf, ripples of ~10–20 cm wavelengths have been observed in storm conditions (Butman et al., 1979). These features are large compared to the acoustic wavelength employed here (1.6 cm), and therefore unlikely to contribute to Bragg scattering. They could, however, modulate the effective incidence angle. On the other hand, Butman et al. (1979) found the seafloor in these regions to be unrippled in calmer conditions.

2.2. Velocity, attenuation, density and porosity

The dependence of bulk physical properties on sediment grain size is described by Hamilton in several papers (e.g., Hamilton, 1972; Hamilton and Bachman, 1982; and references therein). As mean grain size increases porosity fraction (p) decreases, while bulk density (ρ) and compressional velocity (V_p) both increase. Biot's model for sound propagation through porous media, as implemented by Stoll (1977), provides the theoretical relationships between the physical and acoustic properties of ocean sediment. The acoustic–physical property interrelationships for fast and slow waves are given by the frequency equation (Stoll, 1977):

$$\begin{vmatrix} Hk^2 - \rho_B\omega^2 & \rho_W\omega^2 - Ck^2 \\ Ck^2 - \rho_W\omega & m\omega^2 - Mk^2 - j\frac{\omega F\eta}{\kappa} \end{vmatrix} = 0, \quad (3)$$

where H, C and M are Biot complex moduli which are functions of the bulk moduli for the sediment grains, pore water and sediment frame, the shear modulus of the sediment frame and porosity. The frame shear and bulk moduli are treated as complex to account for dissipation at grain contacts. The other variables and parameters in the frequency equation are frequency ω, permeability κ, wet-bulk density ρ_B, pore water density ρ_W, pore water flow parameter m and the complex correction factor F which corrects the pore fluid viscosity η for deviation from Poiseuille flow.

The wet-bulk density is given by

$$\rho_B = \varphi\rho_W + (1-\varphi)\rho_S, \quad (4)$$

where φ is the sediment porosity and ρ_S is the density of the sand grains. The solutions to the frequency equation are the complex wavenumbers of the fast and slow waves which have the form

$$k = \frac{\omega}{V} - i\alpha, \quad (5)$$

where V is the phase speed (m/s), α is the attenuation (nepers/m) and $i = \sqrt{-1}$.

Biot theory (Ogushwitz, 1985) is consistent with experimental data (Hamilton and Bachman, 1982) in predicting that compressional wave velocity decreases with increasing porosity/decreasing grain size until a porosity of ~0.75–0.8, above which compressional wave velocity increases with increasing porosity.

Acoustic attenuation displays a complex grain size dependency (Hamilton, 1972), first increasing and then decreasing as a function of mean grain size, with a peak between ~25 and ~100 μm. Hamilton (1972) hypothesized that attenuation in unconsolidated sediments was a result of loss due to frictional sliding between grains in contact. The Biot model (Stoll, 1977) has performed well for predicting attenuation below 50 kHz (Williams et al., 2002) by including viscous losses for pore fluid motion with respect to the sediment frame and by making the shear and bulk moduli for the sediment frame complex to account for energy dissipation at grain contacts. Williams et al. (2002) compared measurements of attenuation and compressional wave velocity at the Fort Walton Beach sediment acoustics experiment in 1999 (SAX-99) with Biot model predictions of the acoustic sediment properties. The experimental data and theoretical results agreed except that the Biot model underestimated compressional wave attenua-

tion above 50 kHz where scattering losses started to exceed the losses from intrinsic attenuation. Yamamoto (1983) used the Biot model to show that attenuation (dB/m) reaches a maximum when the following condition is met:

$$\frac{\kappa\omega}{2\pi\varphi\eta} \approx 0.1 \tag{6}$$

For a sediment with a given porosity and mean grain size, Yamamoto and Turgut (1988) show that the standard deviation of the sediment pore size distribution can have a significant effect on fast, slow and shear wave attenuation. Fast wave attenuation coefficient versus mean grain size curves, generated with a pore size standard deviation of 1.0 ϕ, agreed with the attenuation measurements reported by Hamilton (1972). The peaks of the attenuation coefficient curves are in the range of 2.0–5.0 ϕ, consistent with Hamilton's in situ data.

2.3. Vertical-incidence reflection

The chirp sonar records the reflection coefficient of the sediment–water interface at normal incidence to the seabed. The reflection coefficient of a flat seabed can be related to the physical properties of the sediments using the Biot model. Chotiros (1994) showed that averaging the backscattered intensity of the sediment–water interface echoes from a rough sea over several transmissions yields the unbiased estimate of the backscattered intensity of a flat bottom if the beamwidth is sufficiently wide. If the beamwidth is too narrow, the average intensity will be less than that generated by a flat seabed due to energy scattering out of the main acoustic lobe of the sonar. In general, the accuracy of estimating the unperturbed reflection coefficient improves with decreasing sonar altitude and decreasing frequency.

The relationship between the reflection coefficient of the seabed at normal incidence and the physical properties is provided by the Biot model (Stoll and Kan, 1981). Chotiros et al. (2002) showed that the reflection coefficient predicted by Biot model agrees with measurements and that the commonly used viscoelastic model overestimates the reflection coefficient by 1–2 dB. Nevertheless, the trends that the model predicts are still valid; i.e., the reflection coefficient increases with decreasing porosity (increasing velocity and bulk density). Because of the general trend between increasing grain size and decreasing porosity, the reflection coefficient is also expected to increase with increasing grain size.

3. Data

The New Jersey shelf has been surveyed extensively with a variety of techniques and for a variety of purposes. Seismic reflection data acquisition has included deep penetration (~10 km) oil industry data (Fulthorpe and Austin, 1998), intermediate penetration (~1 km) seismic data for Ocean Drilling Program site survey (Austin et al., 1996), and a variety of shallow penetration (~30 m) systems such as 3.5 kHz (Twichell et al., 1985; Milliman et al., 1990; Duncan and Goff, 2001), Huntec boomer (Davies et al., 1992, Duncan et al., 2000), and both hull mounted and deep towed chirp (Austin et al., 2001; Nordfjord et al., 2002; A. Turgut, personal communication). Navy interest in this area as a natural laboratory has been long-standing, including a number of acoustic experiments (Pace and Jensen, 2002; Makris et al., 2002). Numerous vibracores have been collected in this area (Buck et al., 1999; D. Lavoie, personal communication) and, in 2002, the AHC800 shallow drilling system was first deployed here to obtain cores in excess of 10 m (Nordfjord et al., 2002; Fulthorpe et al., 2002). The focus in this report is on data pertaining to seafloor characterization, including: multibeam backscatter data, grain size distribution from grab samples, porosity measurements from short cores, seafloor reflection coefficient computed from chirp data, and velocity and attenuation measurements from the In Situ Sound Speed and Attenuation Probe (ISSAP) developed at the University of New Hampshire (Mayer et al., 2002; Kraft et al., 2002). Table 1 summarizes all station values described below.

3.1. Bathymetry and sidescan

Swath bathymetry and sidescan data (Fig. 2) were collected in 1996 as part of the ONR's STRATAFORM program (Mayer et al., 1996; Goff et al., 1999). The survey was conducted using a Simrad EM1000 sonar system aboard the *CHS Creed*. The EM1000 operates at 95 kHz (1.6 cm wavelength) and

Table 1
Measured physical and acoustic parameters at station locations

Longitude	Latitude	Type[a]	c (%)	f (%)	μ_a (ϕ)	σ_a (ϕ)	μ_s, (ϕ)	σ_s (ϕ)	BS (dB)	V_p (m/s)	α (dB/m)	R (dB)	φ
−73.06712	39.35746	S	1.9	1.8	1.20	1.16	1.25	0.70	−26.6	1788	21.1	–	–
−73.05916	39.35378	S	8.8	2.2	0.72	1.62	1.11	0.70	−25.5	1791	32.3	–	–
−73.04288	39.34425	S	0.2	1.2	1.56	0.73	1.53	0.47	−28.7	1756	17.5	–	–
−73.01428	39.32856	O	2.2	5.2	2.13	1.31	2.06	0.53	−26.9	1721	18.4	−9.29	–
−73.00264	39.32163	O	8.4	4.3	1.14	1.75	1.36	0.66	−24.5	1715	63.7	−8.69	–
−72.99076	39.31561	S	3.2	1.1	1.05	1.09	1.19	0.54	−25.5	1755	23.4	−9.10	–
−72.97992	39.30985	S	1.7	0.9	1.09	1.01	1.18	0.62	−30.0	1764	9.2	−9.40	–
−72.97128	39.30497	S	4.9	0.6	1.04	1.15	1.24	0.55	−25.5	1763	28.8	−8.77	–
−72.96692	39.30257	S	1.8	0.2	1.05	0.90	1.16	0.59	−28.7	1756	26.0	−8.77	–
−72.96223	39.29939	S	0.7	0.6	1.19	0.81	1.23	0.56	−27.5	1756	30.5	−8.87	–
−72.95636	39.29706	S	1.3	2.1	1.31	1.04	1.28	0.60	−28.5	1759	10.9	−9.15	–
−72.93417	39.28428	R	0.7	0.7	1.58	0.71	1.58	0.46	−27.5	1756	23.1	−9.09	–
−72.91386	39.27321	R	1.2	1.6	1.66	0.90	1.66	0.43	−28.9	1726	9.5	−9.35	–
−72.90505	39.26868	R	12.4	7.9	1.41	2.20	1.79	0.71	−24.1	–	–	−9.09	–
−72.90001	39.26260	R	2.9	1.1	1.29	1.07	1.40	0.53	−25.3	1749	33.9	−8.90	–
−72.89040	39.26072	R	0.6	0.7	1.74	0.64	1.74	0.39	−30.1	1732	23.3	−9.31	–
−72.87821	39.26906	R	0.2	4.6	2.03	0.99	1.86	0.43	−29.1	1733	25.0	–	–
−72.87130	39.26835	R	5.0	7.6	1.91	1.69	1.87	0.54	−26.0	1710	41.0	–	–
−72.87709	39.25310	R	8.6	8.9	1.68	2.00	1.77	0.58	−24.1	1745	50.0	−9.40	–
−72.86695	39.25195	R	2.2	9.7	2.05	1.54	1.74	0.50	−26.2	–	60.8	−9.52	–
−72.80180	39.27820	R	7.2	3.5	1.24	1.67	1.56	0.64	−25.1	1717	–	–	–
−72.80710	39.26879	R	4.5	3.3	1.40	1.52	1.53	0.75	−26.9	1730	39.2	–	–
−72.83306	39.25441	R	7.5	3.5	1.15	1.63	1.38	0.69	−26.0	1750	29.0	–	–
−72.84438	39.23430	R	12.0	7.1	1.34	2.01	1.60	0.68	−26.9	1715	35.7	−9.52	–
−72.82398	39.22202	O	0.1	2.5	1.65	0.97	1.56	0.62	−29.7	1724	26.7	−9.40	–
−72.78638	39.23865	O	3.3	5.0	1.75	1.57	1.76	0.85	−26.2	1727	33.6	–	–
−72.80183	39.21087	O	15.1	6.2	0.75	2.27	1.40	0.90	−23.5	1714	35.9	−9.47	–
−72.77320	39.19547	O	27.4	3.4	0.49	2.48	1.84	0.84	−23.6	1749	49.5	−9.18	–
−72.75375	39.20313	O	8.7	14.4	2.09	2.31	2.04	0.93	−27.4	1653	38.6	−9.66	–
−72.74675	39.17988	H	1.7	13.6	2.00	1.87	1.53	0.79	−28.9	1674	33.7	−9.80	–
−72.71670	39.16353	H	3.8	13.2	1.80	2.04	1.43	0.88	−30.3	1704	37.1	−10.47	0.46
−72.84603	39.00308	O	2.5	5.5	1.00	1.64	1.00	0.76	−28.3	1745	31.1	−9.59	–
−72.88406	39.02452	O	2.2	2.7	0.87	1.37	0.95	0.78	−26.3	1755	43.3	−9.18	–
−72.90887	39.03753	S	0.5	1.5	1.35	0.94	1.30	0.68	−29.4	1727	20.7	−9.49	–
−72.92272	39.04514	S	2.9	1.6	0.88	1.33	1.07	0.78	−26.3	1781	29.6	−9.14	–
−72.93636	39.05304	S	0.1	1.5	1.38	0.91	1.33	0.68	−29.8	1737	24.6	−8.96	–
−72.94022	39.05578	R	4.3	5.0	0.79	1.66	0.84	0.75	−25.0	1775	48.2	−8.96	–
−72.94737	39.05885	R	1.6	3.9	1.81	1.31	1.80	0.76	−27.8	1755	30.3	−9.48	0.42
−72.95493	39.06159	H	3.4	10.4	1.91	1.90	1.75	0.85	−25.2	1710	40.1	−9.48	–
−72.96344	39.06724	O	7.2	42.2	3.19	2.81	1.87	1.03	−25.8	1627	22.5	−9.45	–
−72.96965	39.05987	O	14.3	14.8	1.34	2.64	1.57	0.86	−23.5	1736	39.3	–	–
−72.97109	39.07106	O	9.3	12.7	1.73	2.32	1.80	0.84	−25.5	1663	32.7	−9.45	–
−72.97994	39.07634	R	1.7	9.5	2.27	1.61	2.05	0.75	−28.3	1714	34.5	−9.72	–
−73.00513	39.09066	R	13.3	7.8	1.08	2.25	1.46	0.88	−24.3	1743	46.4	−9.03	–
−73.00933	39.09343	R	4.8	2.9	1.04	1.47	1.16	0.77	−29.4	1707	18.8	−9.45	–
−73.01408	39.09523	R	0.8	8.5	2.01	1.60	1.80	0.82	−26.6	1710	47.0	−9.30	–
−73.01793	39.09733	R	0.3	2.8	1.41	1.06	1.31	0.65	−28.1	1781	27.7	−9.56	–
−73.02328	39.10091	R	2.0	8.5	2.26	1.49	2.04	0.66	−27.3	1712	33.4	−9.56	–
−73.03338	39.10555	R	3.4	4.3	1.37	1.48	1.38	0.70	−27.4	1746	41.4	−9.41	–
−73.03365	39.10637	R	0.7	1.3	1.70	0.78	1.68	0.47	−30.3	1768	9.1	−9.41	–
−73.10664	39.14527	R	0.1	2.2	1.68	0.86	1.61	0.52	−28.0	1754	16.1	−8.26	–
−73.11005	39.14711	R	13.9	3.1	0.88	2.05	1.61	0.80	−24.6	1742	33.1	−8.26	–

(continued on next page)

Table 1 (*continued*)

Longitude	Latitude	Type[a]	c (%)	f (%)	μ_a (ϕ)	σ_a (ϕ)	μ_s, (ϕ)	σ_s (ϕ)	BS (dB)	V_p (m/s)	α (dB/m)	R (dB)	φ
− 73.12915	39.11696	O	18.8	5.5	0.81	2.28	1.53	0.78	− 21.6	1761	37.1	–	–
− 73.07520	39.10301	R	12.3	6.7	1.29	2.22	1.80	0.79	− 25.2	1757	46.6	–	–
− 73.08653	39.10009	R	1.8	2.6	2.08	1.12	2.09	0.57	− 28.2	1704	15.2	–	–
− 73.09556	39.09969	R	7.5	6.6	1.59	1.90	1.74	0.80	− 24.4	1728	32.9	–	–
− 73.11351	39.09952	R	2.1	7.6	2.27	1.45	2.11	0.61	− 27.5	1707	32.3	–	–
− 73.09358	39.05755	R	0.6	0.7	1.52	0.71	1.52	0.50	− 31.3	1755	18.0	–	–
− 73.07922	39.04995	H	1.0	11.7	2.51	1.53	2.13	0.67	− 27.2	1673	41.4	–	–
− 73.05421	39.03689	H	2.7	12.3	2.23	1.75	1.91	0.69	− 27.1	1726	37.6	–	–
− 73.05193	39.03556	O	8.4	12.9	1.03	2.35	1.04	0.73	− 25.4	1729	38.1	–	–
− 73.03603	39.02733	R	2.3	2.6	1.33	1.19	1.33	0.61	− 26.3	1733	38.8	–	0.39
− 73.04579	39.01654	R	9.8	3.5	0.84	1.71	1.14	0.61	− 25.7	1721	38.2	–	–
− 73.07311	38.99951	R	0.8	0.7	1.25	0.82	1.26	0.58	− 29.1	1743	24.2	–	–
− 73.03767	39.11880	O	3.8	1.6	1.16	1.23	1.31	0.63	− 25.4	1782	13.1	− 9.55	–
− 73.03364	39.12893	S	0.1	2.3	1.59	0.84	1.50	0.47	− 29.2	1734	15.9	− 9.33	–
− 73.02840	39.13941	S	5.7	0.7	0.93	1.30	1.23	0.62	− 25.7	1761	29.4	− 8.96	–
− 73.02635	39.15059	S	1.6	7.3	1.60	1.43	1.34	0.60	− 28.5	1762	15.9	− 9.41	–
− 73.01987	39.16327	S	5.9	0.6	0.67	1.30	1.01	0.68	− 25.8	1805	30.8	− 9.16	–
− 73.01167	39.18510	S	0.3	1.3	1.44	0.79	1.41	0.54	− 27.9	1761	11.9	− 9.58	–
− 73.01683	39.19182	S	0.5	1.2	1.32	0.89	1.31	0.60	− 27.5	1778	14.7	–	–
− 73.00164	39.21090	O	55.0	3.5	− 0.80	2.66	1.84	0.65	− 21.2	1669	23.5	–	–
− 72.99628	39.22337	O	69.8	2.7	− 1.49	2.48	1.91	0.67	− 19.3	1663	41.8	–	–
− 72.98976	39.24079	O	1.2	9.2	2.37	1.36	2.07	0.46	− 28.0	1690	41.5	–	–
− 72.88150	39.34612	R	4.3	0.9	1.06	1.27	1.30	0.67	− 26.1	1734	39.0	− 8.32	–
− 72.86891	39.33881	R	0.7	1.9	1.63	0.87	1.59	0.48	− 29.3	1744	16.6	− 8.32	–
− 72.84885	39.32786	R	5.8	4.0	1.32	1.58	1.46	0.67	− 25.3	1716	52.1	− 8.43	0.40
− 72.84573	39.32638	R	0.8	1.6	1.38	0.93	1.36	0.59	− 28.4	1768	19.3	− 8.43	–
− 72.80438	39.30344	R	1.2	6.1	2.06	1.37	1.91	0.70	− 27.5	1700	35.8	− 9.49	0.43
− 72.78042	39.29005	R	9.0	8.4	1.33	2.06	1.50	0.78	− 25.4	1748	24.4	− 9.17	0.46
− 72.76492	39.28188	R	3.0	6.7	1.83	1.60	1.76	0.73	− 28.3	1725	35.3	− 9.26	0.52
− 72.75281	39.27487	O	18.1	6.9	1.21	2.44	1.97	1.01	− 26.4	1689	42.7	− 9.32	0.45
− 72.73883	39.26724	H	2.2	10.3	2.37	1.71	2.17	0.84	− 28.1	1681	41.8	− 9.68	0.45
− 72.66413	39.22727	H	4.3	17.1	2.16	2.18	1.72	0.86	− 29.5	1646	38.4	− 9.72	–
− 72.66032	39.22460	H	0.3	17.0	2.55	1.80	1.90	0.88	− 30.7	1631	41.4	− 9.72	–
− 72.65873	39.22369	H	0.7	16.3	2.50	1.78	1.90	0.80	− 30.5	1630	37.3	− 9.72	–
− 72.61548	39.19975	H	1.0	24.0	2.71	2.07	1.82	0.91	− 31.1	1602	27.0	− 11.35	–
− 72.51075	39.33999	H	0.0	54.7	4.27	1.97	2.22	0.89	− 33.4	1525	20.3	–	0.53
− 72.53287	39.33076	H	3.2	27.5	2.85	2.30	1.96	0.91	− 30.7	1516	13.0	− 13.49	0.44
− 72.60772	39.32274	H	1.1	20.1	2.53	1.99	1.77	0.86	− 30.4	1613	38.4	− 11.04	0.46
− 72.61182	39.32449	H	1.3	18.6	2.46	1.94	1.76	0.82	− 29.9	1622	39.5	− 10.79	0.44
− 72.63123	39.33415	H	2.8	18.1	2.45	2.03	1.90	0.86	− 30.0	1619	36.4	− 10.92	0.45
− 72.64661	39.34104	H	1.5	16.1	2.90	1.69	2.45	0.77	− 29.3	1605	34.7	− 10.99	0.55
− 72.67616	39.35536	H	5.4	11.5	2.65	1.86	2.62	0.55	− 28.2	1635	41.2	− 11.11	0.47
− 72.73384	39.38476	O	1.7	9.3	2.65	1.36	2.42	0.41	− 29.4	1672	41.7	− 10.90	0.49
− 72.75376	39.39385	O	2.8	7.4	2.28	1.46	2.17	0.52	− 26.6	1699	47.3	− 10.40	0.45
− 72.79327	39.41348	S	0.5	0.7	1.31	0.77	1.31	0.57	− 28.7	1752	13.9	− 9.68	–
− 72.81429	39.42331	S	3.9	0.7	0.97	1.15	1.16	0.64	− 24.9	1733	32.3	− 9.45	–

Parameter key: c: coarse fraction >4 mm; f: fine fraction <0.0625 mm; μ_a: geometric mean over full grain size distribution; σ_a: geometric root-mean-square over full grain size distribution; μ_s: geometric mean over sand grain sizes (0.0625–2 mm); σ_s: geometric root-mean-square over sand grain sizes (0.0625–2 mm); BS: backscatter for 95 kHz Simrad multibeam estimated at 45 grazing angle, averaged over a 90×90 m area; V_p: compressional in situ velocity measurements at 65 kHz; α: compressional in situ attenuation measurements at 65 kHz; R: normal-incidence reflection coefficient at 2 kHz, averaged over profile length of ~500 m; φ: fractional porosity.

[a] Sediment types: H="high fine/low coarse"; R="ribbons"; S="sand ridge"; O="other."

provides both multibeam backscatter and bathymetry with a swath width up to 150° (or ~7.5 times the water depth, although typical survey line spacing is ~5 times water depth to reduce edge artifacts). When operated in its shallow water mode (depths <200 m), 60 beams are formed over an angular sector of 150° using a sonar pulse width of 0.2 ms. The bathymetric footprint ranges from ~5% of water depth at nadir, to ~15% at ±60° and nearly 50% at the outer edge of the swath. Vertical resolution is better than 0.5% of water depth, excluding position, attitude and refraction uncertainties. Although sound speed profiles were collected regularly, large spatial variability in water mass within the survey, particularly near the shelf edge, required subjective correction factors to mitigate refraction effects.

Bathymetric data processing included manual editing of obvious artifacts, tide corrections, reduction of refraction errors associated with incorrect water velocity models, and gridding. Backscatter processing included the application of several gain corrections to remove as much dependence on incident angle as possible. These included: (1) Simrad autogain within 25° incidence angle, (2) addition of 20 log(sec(incidence angle)) beyond 25°, and (3) empirical removal of beam pattern residuals. The net effect of these corrections is to convert the backscatter data to an estimate of the equivalent backscatter strength at 45° incidence angle assuming the seafloor responds in a Lambertian manner.

Bathymetric slopes on the New Jersey shelf are very small; generally ≪1°, and rarely >3°. Slope is therefore a minor contribution to backscatter variability, and response to sedimentary properties is the primary influence on the sidescan map (Fig. 2a). Sidescan data are typically very speckled. Comparison to point measurements, such as those derived from grab samples or probes, requires some measure of averaging to generate a stable mean that is representative of the vicinity. Backscatter values presented in this paper are based on a 90×90 m averaging window centered at the location of interest.

3.2. Grain size distribution

Seafloor sediment samples were collected at 98 stations within the NJ STRATAFORM swath survey (Fig. 2) using a Smith-Mcintyre grab sampler (Murdoch and MacKnight, 1994) aboard the R/V *Cape Henlopen* in 2001. Navigation for each grab sample was recorded from differential GPS, with an accuracy of ~±5 m. Earlier grain size analysis by Goff et al. (2000) suggested that coarse fraction (>4 mm), particularly shell hash, constituted a significant fraction of the grain size distribution in water depths >60 m. Because of the possible strong influence that coarse content may have on the backscatter response, we were particularly cognizant to retain large samples sizes (~500–1000 g aggregate over two or more subsamples) so that coarse content could be stably estimated.

Weight percent of fine grain material (<63 μm) was ascertained by wet sieving, and coarse grained percentages in the 2–4 and >4 mm bins were obtained by dry sieving. The remainder of the distribution was estimated through settling tube analysis using a visual accumulation method. Half ϕ bins were computed from 63 to 500 μm, and 1 ϕ bins from 500 to 2000 μm (grain size in millimeter $=2^{-\phi}$). These values were normalized to the total dry sample weight.

The settling tube analysis was very robust. Using four different samples covering a range of sediment types, root-mean-square (rms) variation on mean sand grain size was at most 0.04 ϕ over multiple independent runs on split portions of the same sample. Differences between subsamples from the same grab were slightly higher, with a rms differential in mean sand grain size of 0.09 ϕ over all grabs. Both the >4 mm and <63 μm portions exhibited rms differential of 3.4%, and 1.4% for the 2–4 mm portion.

Sedigraph analysis of some of the finer-grained grabs indicates that the mean grain size of the <63 μm fraction is typically ~6 ϕ, so this value was assumed for the <63 μm histogram bin in the computation of whole-distribution mean and rms grain sizes (Table 1). Our sample sizes for the >4 mm fraction precluded accurate quantification of those grain sizes. For this histogram bin size, we assumed a mean grain size of −3 ϕ.

3.2.1. Parameterization of grain size distribution

Grain size histograms displayed in Fig. 3 typify much of the sediment sampled on the New Jersey mid- and outer shelf. While some samples display unimodal behavior, either symmetric (Fig. 3a,c) or

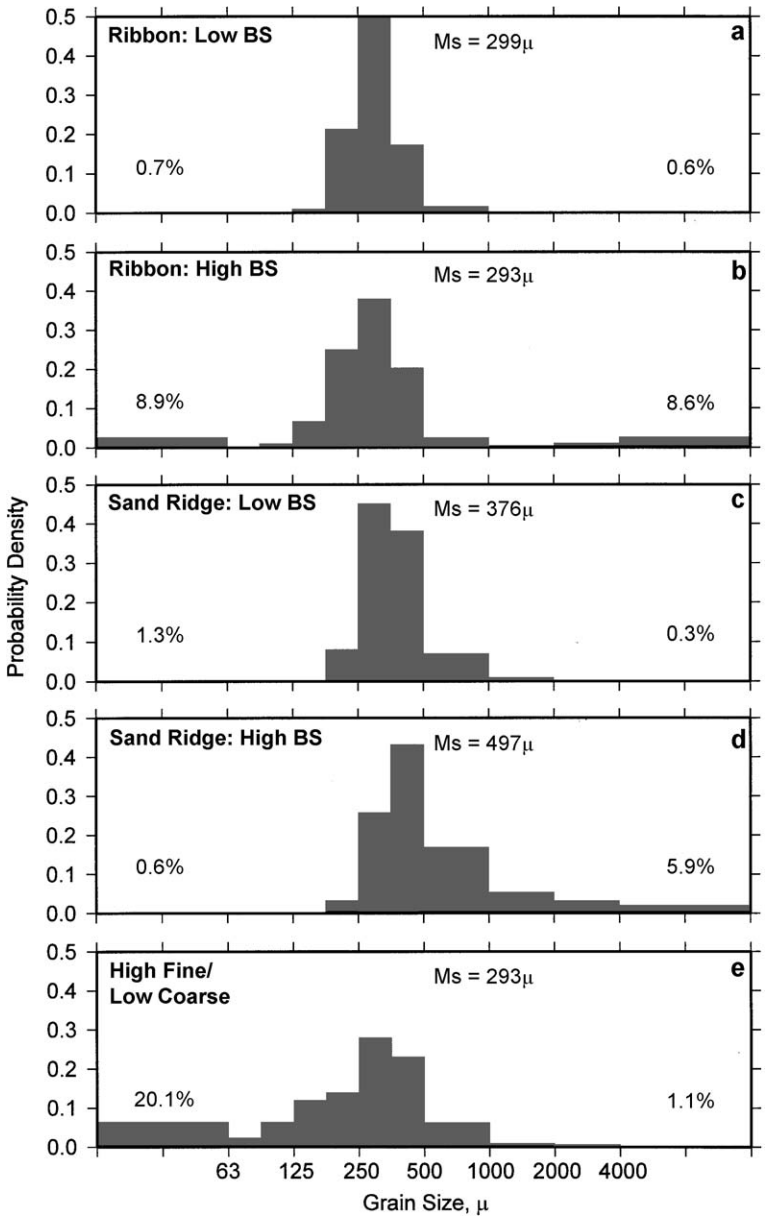

Fig. 3. Example grain size histograms covering a range of sediment types and relative backscatter (BS) intensities. Values indicate fine % by weight <63 μm, mean sand grain size (Ms), and coarse % >4000 μm.

skewed (Fig. 3d), others are either bimodal (Fig. 3e) or even trimodal (Fig. 3b), with significant contributions in either the fine or coarse bins. Grain size histograms are typically parameterized with unimodal distribution properties: mean, rms, skewness and kurtosis (Pettijohn et al., 1987). While these parameters (mean and rms are given in Table 1) could be used to quantitatively distinguish the histograms shown in Fig. 3, they are ultimately unsatisfactory because they fail to reveal directly the important physical properties of the sediments. For example, the grain size histograms of Fig. 3a,b, with nearly

identical means, could be distinguished by their differences in rms and kurtosis. However, these values do not adequately emphasize the complex nature of the distribution; i.e., that in addition to the medium sands, there is also nearly 9% each of fine- and coarse-grained material in one (Fig. 3b) but not the other (Fig. 3a). Furthermore, lack of grain size resolution in the <63 μm and >4 mm bins makes it difficult to robustly define an overall mean, variance, skewness or kurtosis when significant portions of these grain sizes are present. In this paper, we instead employ the mean sand grain size (computed over 63–2000 μm), coarse % and fine % as our primary descriptors of the grain size distribution (Table 1). Histograms of these parameters over all samples gathered are displayed in Fig. 4a–c. Over all samples, coarse % is largely independent of either mean sand grain size (correlation coefficient, $\rho = 0.08$) or fine % ($\rho = -0.06$). Mean sand grain size and fine % are moderately correlated with each other ($\rho = 0.49$, for grain size specified in ϕ values).

3.2.2. Visual check on coarse %

The ISSAP instrument (see below) included a video camera, installed primarily for the purpose of confirming the insertion of the transducer probes into the seafloor. Although the quality of the recorded images was fairly poor, the visual data are useful for a qualitative assessment of shelly material resting on the seafloor (Fig. 5). We were also unable to observe any ripples in these images.

At each station, the seafloor was categorized as either "very shelly", "fairly shelly", "somewhat shelly", "few shells" or "no shells" based on a subjective assessment of several video stills. For the great majority of stations, the weight percentage of

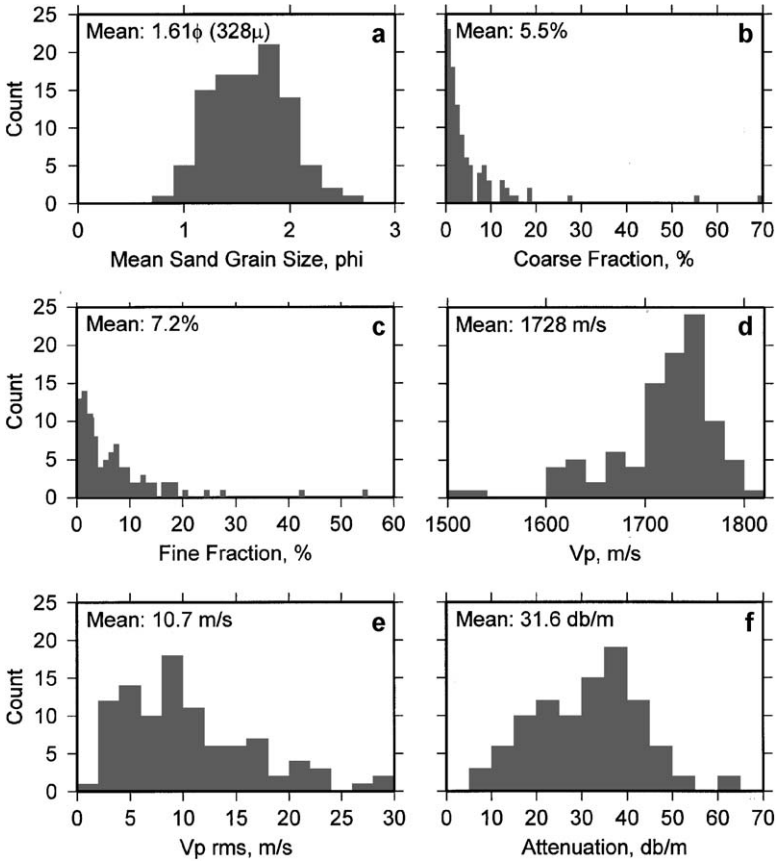

Fig. 4. Histograms of various sediment parameters measured for analysis.

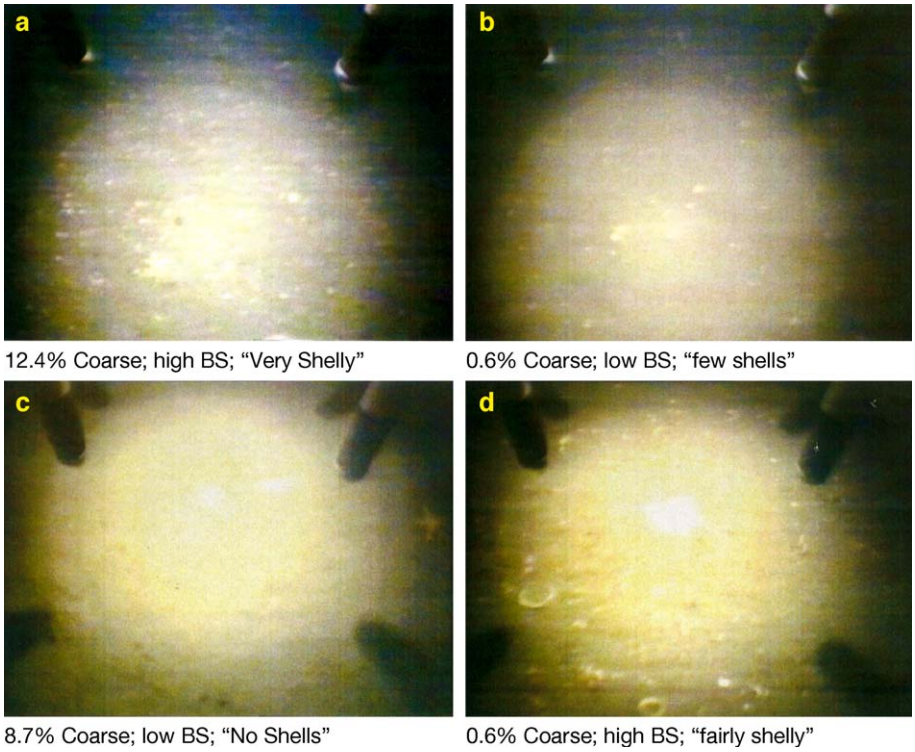

Fig. 5. Images captured from video data collected during ISSAP deployment. Images (a) and (b) show a typical case where high or low measured coarse % correspond well to qualitative characterizations of shelly material on the seafloor as well as indications of high or low backscatter (BS). Images (c) and (d) are examples of occasional situations where there is, respectively, either too much or too little coarse % sampled given both the images and the backscatter measurements.

coarse material corresponded well to the visual evidence (e.g., Fig. 5a,b), indicating that the coarse % measurement is generally representative of material resting at the seafloor. However, a number of anomalies were present, such as areas of no evident shells where significant shell material was recovered (Fig. 5c), or shelly areas where little coarse material was recovered (Fig. 5d). The grabs are thus commonly but not always representative of the coarse material seen at the seafloor. We surmise that the distribution of shell material is not perfectly even; i.e., that in a shelly region, it is possible to hit a spot with a grab sampler that is relatively devoid of shells, and likewise in a region of few shells it is possible to hit a pocket of shelly material.

We demonstrate in the following section that backscatter is, for the most part, primarily correlated with coarse %. However, where there was a discrepancy between measured coarse % and qualitative visual evidence of coarse material at the seafloor, the latter was a better gauge of backscatter.

3.2.3. Partition into sediment categories

A geologic assessment of the STRATAFORM area based on the geomorphology (Goff et al., 1999) and grab sample grain size distributions lead us to distinguish three categories of bottom types (Fig. 2; Table 1).

"Ribbons" are alternating bands of high and low backscatter oriented NE–SW, parallel to the mean currents and typically lying in wide, erosive swales oriented in the same direction (Goff et al., 1999). Samples and short cores indicate that the high backscatter areas are composed primarily of medium sand mixed with significant portions of shell hash and fine grained sediment (Fig. 3b). The lower backscatter areas are well-sorted medium sands (Fig. 3a) which overlie the shelly/muddy sands in a layer a few tens of

centimeters thick. There are 40 sample stations in the "ribbon" category.

"Sand Ridges" are large bedforms (~1–4 km wide; ~2–10 km long; ~2–6 m high) oriented oblique to the regional contours (typically ~30°). Formed in a near shore environment (e.g., Swift and Field, 1981), sand ridges continue to be modified up to water depths of ~50 m (Rine et al., 1991; Snedden et al., 1994, Goff et al., 1999). In the water depths considered here, sand ridges are likely moribund, but subject to gradual winnowing (Goff et al., 1999). Here, sand ridges exhibit a consistent pattern of higher backscatter on the ridge tops and lower backscatter in the lows. Sand ridges are composed primarily of well-sorted medium to coarse sand (Fig. 3c,d), with some significant shell content. There are 20 sample stations in the "sand ridge" category.

The "high fine/low coarse" samples are defined as having >10% fine and <5% coarse grained sediment (or no shells as seen in video stills). For the most part, these stations come from the area known as the Hudson Apron, a promontory of the shelf edge to either side of the Hudson Canyon (Fig. 1; Ewing et al., 1963; Knebel, 1979; Twichell et al., 1985). The seafloor in this area is remarkable for the preservation of iceberg scours (Fig. 2b), evidently formed in the early Holocene (Goff et al., 1999; Duncan and Goff, 2001). Stiff clays in the shallow subsurface preserve the scour morphology. Three other examples in this category are sampled in what appear to be erosional pits. There are 17 sample stations in the "high fine/low coarse" category.

There are 21 grab stations of "other" sediment types that do no fit within the above categories. Six of these are from gravelly areas that produce some of the highest backscatter in the region (Fig. 2).

3.3. ISSAP data

The ISSAP device was developed and built by the University of New Hampshire's Center for Coastal and Ocean Mapping (Mayer et al., 2002; Kraft et al., 2002). Grab sampling and ISSAP deployment were conducted during the same cruise and occupied the same set of stations. The ISSAP employs four transducer probes inserted ~15 cm into the seafloor sediment, obtaining five independent transmit/receive paths over a nominal probe spacing of 20–30 cm. The operating frequency is ~65 kHz. The recorded waveforms were processed for sound speed using both cross-correlation and envelope detection methods, and for sediment attenuation using the filter-correlation method (Courtney and Mayer, 1993; Kraft et al., 2002). Data collection is reliable and precise, with single path variability of only ±1–2 m/s for sound speed and <±1 dB/m for attenuation. Between paths, however, more significant variability of up to ±30 m/s at a number of stations is observed. Histograms for compressional velocity, single station rms for compressional velocity, and attenuation are displayed in Fig. 4d–f. The velocity values listed in Table 1 tend to be smaller than values determined by Hamilton and Bachman (1982) from laboratory samples, but are comparable to Hamilton's (1972) in situ measurements.

3.4. Resistivity-based porosity

A hydraulically damped gravity corer was used to collect 18 undisturbed samples (Fig. 2) for sediment physical property measurements. This device, henceforth referred to as the "slow corer", advances a 1-m-long, 15-cm-diameter polycarbonate barrel into the seabed under a 350-kg weight package countered by a hydraulic piston. A controlled, slow rate of entry (10 cm/s in this study) minimized disturbance to the sediment–water interface and fine-scale stratigraphy. Typical penetration depths were 20 – 50 cm in sands and consolidated muds, though the corer was ineffective in shell-layered bottoms that characterize much of the New Jersey middle shelf.

Profiles of resistivity porosity were measured in the slow cores aboard ship using a four-terminal AC probe modified from the design of Andrews and Bennett (1981). An electronic micromanipulator was used to advance the 6-mm diameter probe into the sediment – water interface at a rate of 1 mm/s, generating profiles at 1-mm depth resolution. Interconnected porosity was computed from the resistivity data using the well-known relationship:

$$R_s/R_w = \varphi^{-n} \quad (7)$$

where φ is the sediment porosity (ratio of the volume of void space to the total volume of sample), R_s is the resistivity of the saturated bulk sediment, R_w is the

resistivity of the interstitial fluid, and n is a sediment-specific empirical constant (Jackson et al., 1978). It was assumed that the resistivity of bottom water was equivalent to that of underlying pore waters, so R_w was taken as the average resistivity $0-5$ cm above the sediment–water interface in cores. A value of $n=1.5$ was found to be most representative for New Jersey shelf sediments and was employed in all cases.

In situ resistivity porosity values for the seabed (ex situ in the case of slow cores) have potential to be higher than those determined gravimetrically from split cores and grab samples. One cause for disparity is drainage and (or) minor desiccation during sample handling which, by decreasing the water content, decreases computed porosity. Measurement geometry is another consideration; because porosity decays most rapidly near the sediment–water interface, porosity values integrated over several decimeters below the interface (e.g., Hamilton and Bachman, 1982) will necessarily be lower than those measured discretely with a small-diameter probe. For the purpose of comparing porosity to other physical and acoustic properties, porosity values $2-6$ cm below the sediment–water interface were averaged to attain a mean considered representative for the seabed.

3.5. Chirp reflection coefficient

A chirp sonar, designed and fabricated by Florida Atlantic University, measured acoustic reflections at normal incidence to the seabed using a dual pulse technique to produce high-resolution imagery of near-surface sediments and lower resolution imagery of deeper sediments. A 40-ms-long FM pulse with a band of 1.5–4 kHz was transmitted to provide imagery of the top 40 m of the seabed with a vertical resolution of 40 cm, while a 10-ms-long FM pulse with a band of 1.5–15 kHz was alternately transmitted to yield 10-cm resolution imagery of sediments in the top 10 m. In the sonar vehicle, two Tonpilz-type piston sources with operating bands of 1–5 and 4–16 kHz were driven simultaneously to generate the wide-band output pulses. The seabed reflections were measured by a horizontal, 1-m-long by 1-m-wide planar hydrophone array.

The absolute reflection coefficient of the sediment–water interface was determined from the ratio of the echo energies produced by the seabed and an air–water interface. The echo energy of the air–water interface was measured in a mineral spring in which the chirp sonar vehicle was inverted to collect normal incidence reflection echoes from the air–water interface. The mineral spring, located in Southwest Florida, provided a mirror-like surface yielding a ping to ping standard deviation at least 40 dB below than the average echo intensity.

The reflection data are calibrated at the low end of the frequency band because the wider beamwidth of the hydrophone array makes the reflection coefficient measurement less susceptible to sonar vehicle motion and the longer wavelength reduces error associated with seabed roughness. The New Jersey shelf chirp data are calibrated at 2100 Hz by passing both the matched-filtered seabed reflection data and the mineral spring reflection data through a band-pass filter with a bandwidth of 500 Hz and calculating the reflection coefficient with the expression,

$$R=\sqrt{\frac{\left\langle (c_2t_2)^2\int_{t_2-T/2}^{t_2+T/2}s_2(t)s_2^*(t)\mathrm{d}t\right\rangle}{\left\langle (c_1t_1)^2\int_{t_1-T/2}^{t_1+T/2}s_1(t)s_1^*(t)\mathrm{d}t\right\rangle}} \tag{8}$$

where t_1 and t_2 are the respective arrival times of the band-pass filtered and matched filtered air–water interface echo $s_1(t)$ and the bottom echo $s_2(t)$, T is the width of the energy gating window, which is approximately equal to twice the inverse of the bandwidth of the band-pass filter, and c_1 and c_2 are the water sound speeds for the mineral springs and seawater, respectively. The asterisk indicates the complex conjugate of the analytic signal. The brackets $\langle\ \rangle$ indicate averaging over several transmissions.

The reflection data reported in Table 1 are based on the average energy of seabed echoes that met the criteria of a ping to ping standard deviation at least 23 dB below the average reflection coefficient. The ping-to-ping standard deviation is measured every 20 transmissions which corresponds to approximately 25 m along track distance. The threshold of 23 dB is a tradeoff between having sufficient data for averaging and incorporating more data with greater noise levels

and larger biases caused by inhomogeneities at or near the sediment–water interface causing errors in the reflection coefficient measurement. The reported values represent an average taken over a profile distance of ~500 m, which is large compared with many of the variations in sedimentology exhibited by the side-scan data (Fig. 2a).

4. Correlation analysis

In this section, we explore the empirical relationship between backscatter, parameters of the grain size distribution, compressional velocity and attenuation, and, where available, porosity. Strong correlations between parameters are commonly exhibited as approximately linear relationships easily discerned by eye. Where appropriate, we quantify our observations using the Pearson's correlation coefficient, ρ (Press et al., 1986). Nearly all quoted coefficients of absolute value >0.40 are statistically different from zero at greater than 99% confidence.

4.1. Backscatter versus grain size distribution

Acoustic backscatter is compared to parameters of the grain size distribution in Fig. 6. Backscatter exhibits a strong but nonlinear dependence on the coarse % (Fig. 6a). This dependence is made even more robust by removing from consideration those samples for which the amount of coarse material in the grab sample was inconsistent with visual evidence

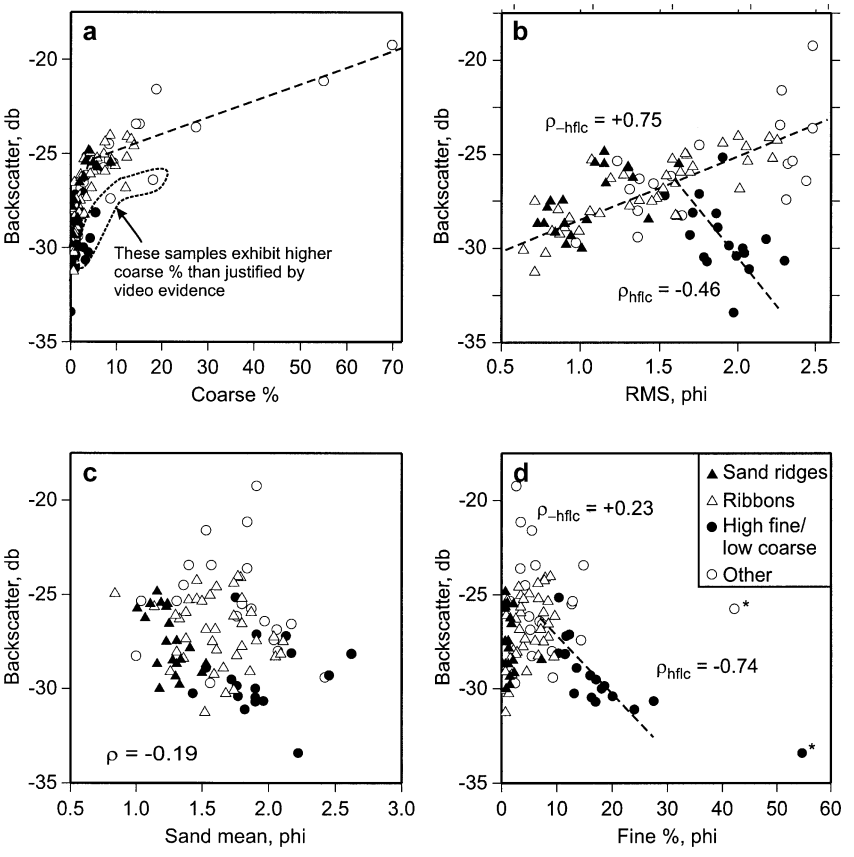

Fig. 6. Backscatter values plotted versus parameters of the grain size distribution. Symbols distinguish different sediment types as described in the text. The parameter ρ_{hflc} indicates the correlation coefficient over the "high fine/low coarse" sediment population, and $\rho_{-\mathrm{hflc}}$ is the correlation coefficient over the remaining samples. Symbols annotated with an asterisk are considered outliers. Dashed lines highlight evident linear trends.

of coarse material at the seafloor (e.g., Fig. 5c). The strong qualitative relationship with visually observed coarse material implies that the backscattered acoustic energy is derived primarily from the seafloor.

Because of the nonlinearity of this relationship, a correlation coefficient does not adequately represent the codependency of these parameters. However, sediment sorting, quantified by the rms of the full grain size distribution (Table 1), provides an alternative, more linear, and revelatory view of the relationship between backscatter and coarse content (Fig. 6b). Sorting is strongly dependent on the tails of the distribution; i.e., the coarse and fine content. For the most part, sorting and backscatter exhibit a strong positive linear relationship irrespective of sediment type, with one exception: the high fine/low coarse population of samples, which is clearly separate from this trend and displays a moderately resolved negative correlation to backscatter. For the remainder, therefore, we infer that the coarse content is responsible for the strongly linear relationship between sorting and backscatter.

The mean sand grain size is not significantly correlated to backscatter, regardless of sediment category (Fig. 6c). However, with fine % (Fig. 6d), we again see a distinction in the backscatter dependence between the high fine/low coarse category and the rest of the samples. Here, backscatter is well correlated to fine % in the high fine/low coarse population but poorly correlated over the remainder.

4.2. Velocity versus grain size distribution

Compressional wave velocity is plotted against parameters of the grain size distribution in Fig. 7. Here, we observe that velocity is strongly dependent on grain size, correlating positively with mean sand grain size (Fig. 7b; note that higher ϕ indicates lower grain size) and negatively with fine % (Fig. 7c); both results are consistent with prior observations of the dependence of velocity on grain size (e.g., Hamilton, 1972; Hamilton and Bachman, 1982). All sediment categories fall on the same trends in both cases. The two outliers noted in Fig. 7c are derived from locations where stiff, overconsolidated clays are present in the cores below ~10–20 cm of unconsolidated sediment. It is possible that the ISSAP transducer elements transmitted within this more

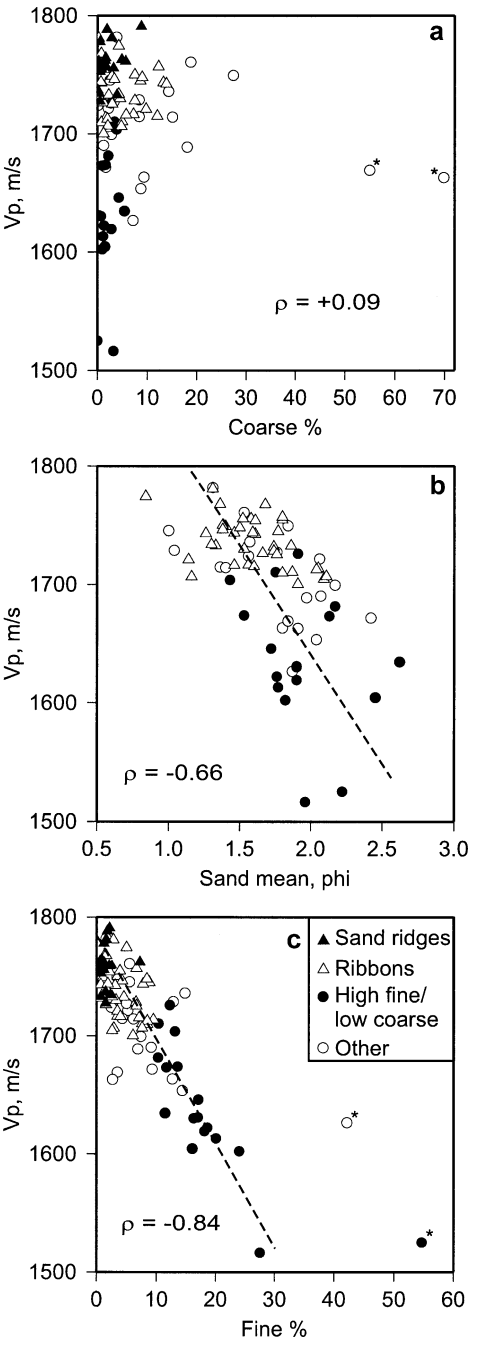

Fig. 7. Compressional velocity (V_p) values plotted versus parameters of the grain size distribution. Symbols distinguish different sediment types as described in the text. The parameter ρ indicates the correlation coefficient over entire population of samples. Symbols annotated with an asterisk are considered as outliers. Dashed lines highlight evident linear trends.

competent material. Measured coarse % does not correlate with velocity to any significant degree (Fig. 7a).

4.3. Attenuation versus grain size distribution

Attenuation is plotted against parameters of the grain size distribution in Fig. 8. Excluding outliers, attenuation shows a minor positive correlation with coarse % (Fig. 8a) and no significant correlation with mean sand grain size (Fig. 8b). The two outliers for the coarse % are both large gravel samples, for which the acoustic measurements are suspect. The relationship with fine % is complex (Fig. 8c). Restricting consideration to fine content <22%, the correlation is moderately positive. We might be tempted to dismiss the samples with greater fine % and low attenuation as outliers, but for the fact that prior results (Hamilton, 1972; his Fig. 3) show that, as a function of grain size, attenuation first rises and then falls, peaking at ~4 ϕ (63 μm). Indeed, when we instead restrict our consideration to samples with fine content >10% (most of which are high fine/low coarse sediment type), the correlation between attenuation and fine % is strongly negative. We have also examined the relationship between attenuation and overall mean grain size, but can discern no clear relationship between the two parameters that could be construed as consistent with Hamilton's results. However, consistent with the primarily positive correlations between attenuation and both coarse

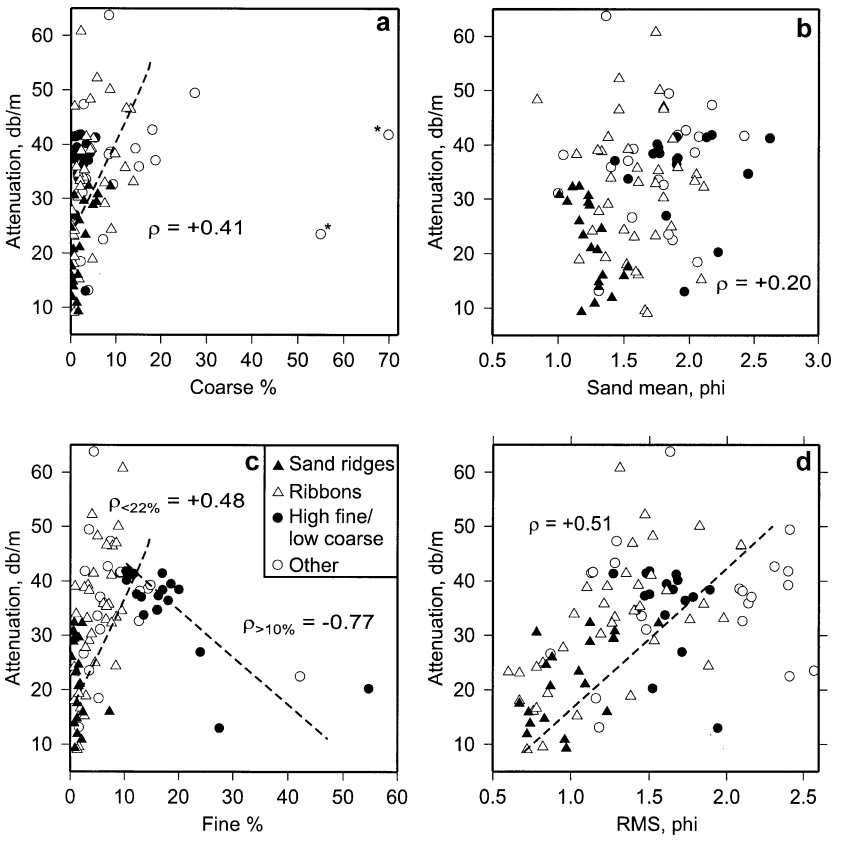

Fig. 8. Attenuation values plotted versus parameters of the grain size distribution. Symbols distinguish different sediment types as described in the text. The parameter ρ indicates the correlation coefficient over entire population of samples. The parameter $\rho_{<22\%}$ indicates the correlation coefficient over the fine fraction <22%, and $\rho_{>10\%}$ likewise indicates the correlation coefficient over fine fraction >22%. Symbols annotated with an asterisk are considered as outliers. Dashed lines highlight evident linear trends.

% and fine %, attenuation displays a moderately positive correlation with rms (Fig. 8d). This latter correlation is consistent with qualitative observations noted by Kraft et al. (2002).

4.4. Backscatter, velocity, and attenuation versus each other

Backscatter, velocity, and attenuation are plotted versus each other in Fig. 9. The correlation between backscatter and velocity (Fig. 9a) is strongly positive for the high fine/low coarse sediments, while poorly if negatively correlated for the rest of the sample population. This relationship is consistent both with the strong negative correlation between velocity and fine % (Fig. 7c) and the negative correlation between fine % and backscatter seen over the high fine/low coarse samples (Fig. 6d). Velocity and attenuation (Fig. 9b) are also positively correlated over the high fine/low coarse sediments, while weakly negatively correlated over the remaining samples. This behavior is likewise consistent with the negative correlation between velocity and fine % and the change in trend between fine % and attenuation noted in Fig. 8c.

Finally, we note that attenuation and backscatter (Fig. 9c) are modestly correlated with each other. This observation is consistent with the modest correlation observed between coarse % and attenuation (Fig. 8c) and the correspondence between coarse % and backscatter (Fig. 6a).

4.5. Porosity

The limited number of core-derived porosity measurements display moderate negative correlations with both backscatter (Fig. 10a) and velocity (Fig. 10b), both expected based on theoretical arguments stated in Section 2. Note that half of the coring stations are coincident with high fine/low coarse samples, so it is

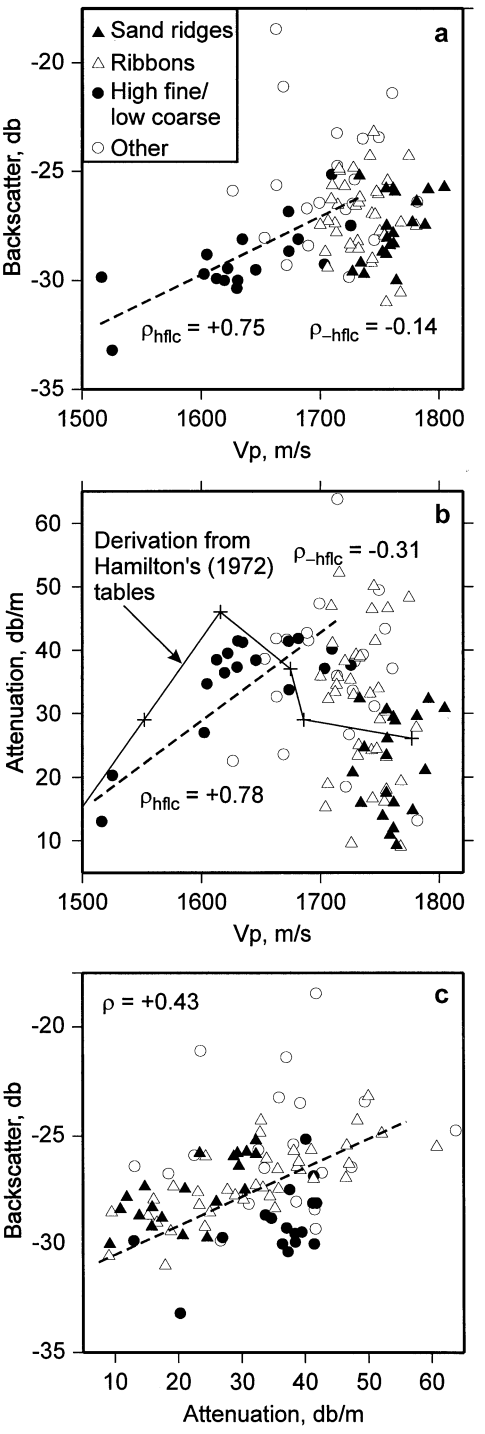

Fig. 9. Plots of (a) backscatter versus compressional velocity (V_p), (b) attenuation versus velocity, (c) backscatter versus attenuation (c), and (d) backscatter versus porosity averaged from 2 to 6 cm within the slow cores. The parameter ρ_{hflc} indicates the correlation coefficient over the "high fine/low coarse" sediment population, and ρ_{-hflc} is the correlation coefficient over the remaining samples. Symbols annotated with an asterisk are considered as outliers. Dashed lines highlight evident linear trends.

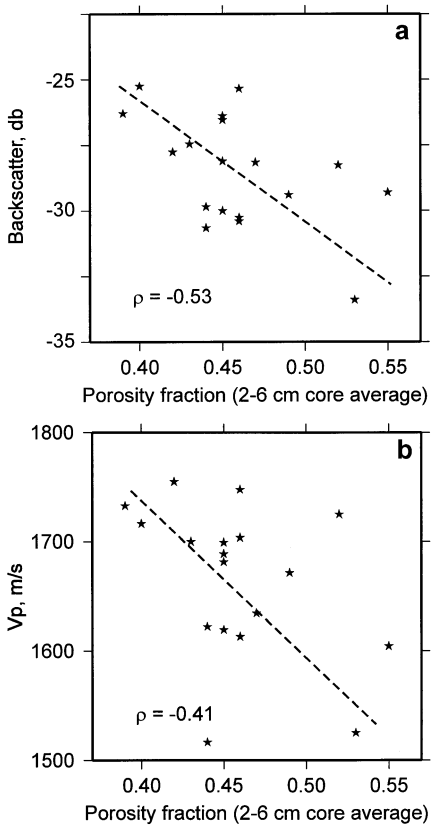

Fig. 10. Plots of (a) backscatter and (b) velocity versus porosity averaged from 2 to 6 cm within the slow cores.

reasonable to infer that much of the correlation evident in Fig. 10a is associated with clear dependence of backscatter at those stations on bulk physical properties rather than on scatter from coarse material at the seafloor.

A thorough examination of porosity versus grain size will be presented in a future study that incorporates complete analysis of the cores.

4.6. Vertical-incidence reflection coefficients

Vertical-incidence reflection coefficients (measured at 2 kHz) are plotted versus in situ velocity measurements (65 kHz) in Fig. 11. The correlation is very strong, confirming the expected relationship between these two parameters. The correlation also indicates a high potential for utilizing vertical-incidence reflection, carefully culled for high-confidence values, for remote-sensing characterization of sediment physical properties.

5. Semi-variogram analysis

We quantify the variability of our measurements as a function of spatial scale by estimating the semi-variogram (e.g., Christakos, 1992; Deutsch and Journel, 1992). For a random function $Z(x)$, the semi-variogram $\zeta(\mathbf{L})$, specified as a function of lag $\mathbf{L}$ (the separation between two points) is defined by the relationship

$$\zeta(\mathbf{L}) \equiv \frac{1}{2} E[(Z(x+\mathbf{L}) - Z(x))^2], \tag{9}$$

where $E[\ ]$ is the expectation operator. In other words, the semi-variogram is half the expected value of the square of the difference between two values separated by lag $\mathbf{L}$. Because of data limitations (see below), we restrict consideration to the isotropic case $L = |\mathbf{L}|$. A purely random field (i.e., white noise) will be specified by a constant value semi-variogram (equal to the variance) for all values of $L>0$. A field that exhibits random but correlatable structure will be specified by a semi-variogram that increases with increasing lag distance. If the semi-variogram levels-off, or "sills" in the geostatistics terminology (e.g., Cressie, 1988), the value of the sill is equal to the variance, and the lag at which the sill begins defines the decorrelation distance (also known as the range) to the morphology. Where

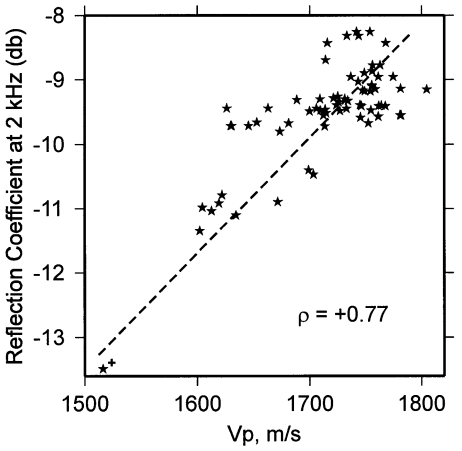

Fig. 11. Vertical-incidence reflection coefficient at 2 kHz versus in situ compressional velocity measurements. The value indicated by the cross represents an assignation of a reflection coefficient to a station ~5 km away from the seismic line, based on assumed similarity of geology at the two locations. Without that value, the correlation is still robustly positive ($\rho = +0.70$).

the variance can be well defined, the semi-variogram is equal to the covariance function subtracted from the variance, which is, in turn, the inverse Fourier transform of the power spectrum.

Estimating the semi-variogram from spatially irregular data, such as the grab sample and ISSAP probe measurements, requires binning and averaging all squared differences that fall within specified ranges of lag distance. Restriction to the isotropic case in our circumstances is required because the number of stations do not provide sufficient bin averaging in two dimensions given the range of scales of interest. Following the methodology developed by Goff et al. (2002) for semi-variogram estimation for randomly distributed data, bin sizes were chosen dynamically such that an equal number of samples fell within each bin (50 samples per bin for the station data). The advantage in this method is that the empirical semi-variogram is equally resolved at each point sampled, and the density of semi-variogram samples is adjusted to the number of data points available to constrain that lag range.

Incorporating all sample stations into the computation of the semi-variogram, our results were dominated by the long-range variance associated with the difference between the Hudson Apron samples (Fig. 2) and the remainder of the survey area. The former are much finer-grained overall and exhibited lower velocities; all of these samples are within the "high fine/low coarse" sediment category. Geologically, this is a unique seafloor exposure, limited in spatial extent to the proximity of the Hudson Apron (e.g., Twichell et al., 1985). The remainder of our samples, an intermixture of sand ridge, ribbon and other sediment types, are more likely to be typical of much of the Atlantic mid- and outer shelf. It is therefore of interest to characterize the spatial variability of this type of seafloor by removing the Hudson Apron samples from our consideration in the estimation of semi-variograms.

Selected semi-variograms computed from the non-Hudson Apron samples are plotted in Fig. 12. These functions display a high degree of uncorrelated random variability. The level of such variability is related to the data variance, decorrelation distance, and amount of data used to estimate the semi-variogram (see discussion of covariance estimation in Goff and Jordan, 1989). Semi-variograms estimated by binning randomly located data typically display a high degree of uncorrelated variability. Not shown in Fig. 12 are semi-variograms for attenuation and fine %, which exhibit nothing but such uncorrelated variability; evidently the random component of variability in these parameters overpowers any structural information. However, in each of the examples shown in Fig. 12, we observe structure to the curve which rises above the level of uncorrelated variability.

The velocity, mean sand grain size, and reflection coefficient semi-variograms (Fig. 12a) increase with lag until ~10–15 km, and remain approximately level thereafter at a variance of ~1100 $(m/s)^2$ for velocity, ~0.125 ϕ^2 for sand grain size, and ~0.16 $(dB/m)^2$ for reflection coefficient. Mayer et al. (2002) determined that, on scales of ~1 km, velocity varies by as much as 100 m/s, while on scales of 10's of kilometers velocity varies by as much as 200–300 m/s. Bearing in mind that peak-to-peak variations are approximately twice the rms, the velocity semi-variogram (Fig. 12a) is broadly consistent with their observations. Scaled appropriately, and taking into consideration the high degree of random variability exhibited by each, the three size semi-variograms in Fig. 12a are closely matched, further supporting the evident relationship between these parameters exhibited by direct correlations in Figs. 7b and 11. This structure can be fitted by the well-known von Kármán (1948) statistical model (e.g., Tatarski, 1961; Wu and Aki, 1985; Frankel and Clayton, 1986; Goff and Jordan, 1988; Holliger et al., 1993; Goff, 1995), which provides useful statistical characterizations through its parameterization. Fitted here simply by eye, we infer a variance, $H^2 = 1000$ $(m/s)^2$ for velocity (0.114 ϕ^2 for mean sand grain size; 0.145 $(dB/m)^2$ for reflection coefficients), characteristic scale, or decorrelation length, $\lambda_\theta = 12.6$ km, and fractal dimension, $D = 2.7$. A "noise spike" of 100 $(m/s)^2$ (0.0114 ϕ^2 for mean sand grain size; 0.0145 $(dB/m)^2$ for reflection coefficients) was also added to match the mean station rms velocity (Fig. 4e).

Like velocity, mean sand grain size and reflection coefficients, the backscatter and coarse % semi-variograms display very similar structure when scaled appropriately (Fig. 12b), reinforcing the direct correlation observed between these two parameters in Fig. 6a,b. The observed structure is, however, quite a bit different than that seen in Fig. 12a. From the smallest sample lag (nearly 1 km) to ~8 km, no discernable

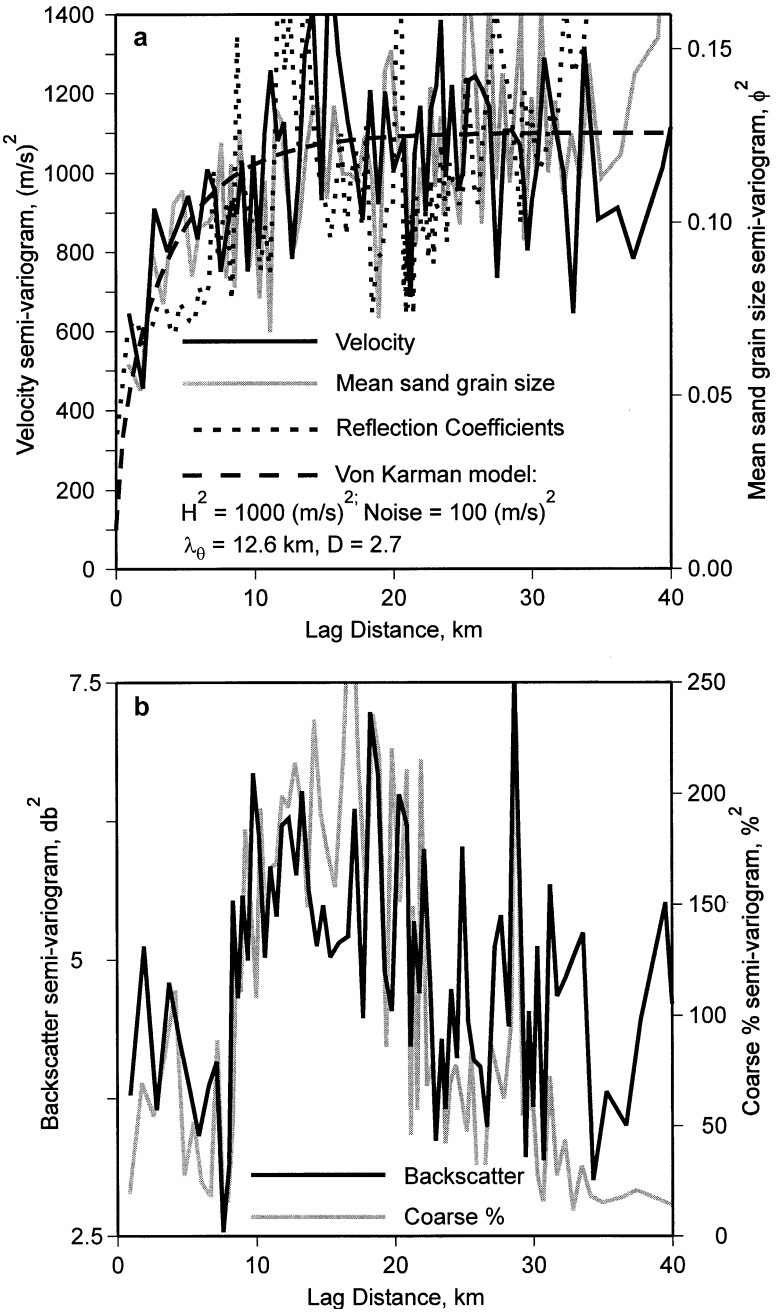

Fig. 12. Semi-variograms computed for (a) velocity, mean sand grain size, and vertical-incidence reflection coefficients at 2 kHz (range of values: 0–0.2 $(dB/m)^2$), and (b) backscatter and coarse %. Samples from the Hudson Apron area were excluded from computation of the semi-variograms because of the large, deterministic change in sediment properties associated with this province. The reflection coefficient semi-variogram was computed from all available values on the seismic lines indicated in Fig. 2, not just those associated with specific station locations.

structure is observed; i.e., variability in these parameters is ''white'' in character over this lag range. Variance then increases abruptly above ~8 km lag. This step-like structure indicates that the spatial variability in backscatter and coarse % is not a continuum of scales, such as seen in fractal media, but rather is a superposition of structures of widely different scales. Such a separation of scales can be seen qualitatively by inspection of the backscatter map (Fig. 2a), where the ''ribbon''-like small scale variability appears distinct from the larger scale variability associated with gravel patches, sand ridges, etc. The backscatter and coarse % semi-variograms decrease abruptly again at ~21 km lag. It is difficult to interpret a reduction in variance with lag, and may be an artifact of the limited sampling of larger-scaled structures.

6. Discussion

6.1. Backscatter

Our study provides strong empirical evidence regarding the sedimentary influences on acoustic backscatter. Over most of the New Jersey middle and outer shelf, backscatter and velocity are unrelated to each other. Rather, backscatter is positively correlated to coarse content, either gravel or shell material on the seafloor, while velocity is positively correlated to sand grain size and negatively to the percentage of fine grained material. However, while coarse content appears to be the major influence on backscatter when sufficient (>5%) coarse material is present, other factors come to the fore when it is not. For example, both velocity and fine % are well correlated with backscatter over the ''high fine/low coarse'' population of sediment samples in this study. Also, in a study of grain size distribution in the shallower (~20–40 m water depth) portions of the STRATAFORM survey, Goff et al. (2000) observed strong correspondence between variations in backscatter and variations in mean grain size in well-sorted, medium grained sands without significant coarse content. Although velocity measurements were not gathered during that study, we can infer from Fig. 7b and from Hamilton and Bachman's (1982) figures that velocity varied in kind with the changes in mean grain size.

The observations noted above highlight the importance of considering both grain size roughness and bulk properties in ground truthing acoustic backscatter. They also underscore the evident importance of the Bragg wavenumber to scattering (Eq. (1)). Where seafloor grain size is well below the Bragg wavelength, roughness on the scale of the Bragg wavelength is very small, and not dependent on variations in grain size. Backscatter under these circumstances correlates primarily with bulk properties, i.e., the function dependence $F(\theta,v,\rho)$ in Eq. (1). However, with even a minor portion (5–10%) of shell hash or gravel, whose roughness properties are on the order of the Bragg wavenumber, backscatter becomes dominated by the abundance of such features, i.e., the $W(2k_a\cos\theta,0)$ dependency in Eq. (1).

6.2. Attenuation

Attenuation displays a marked change in trend as a function of both fine % and velocity, first rising and then falling (Figs. 8c and 9b). We assume that this response is associated with intrinsic attenuation, rather than scattering attenuation; the latter may be related to the evident correlation between attenuation and coarse % (Fig. 8a). The complex relationship between attenuation and fine % and velocity is similar to Hamilton's (1972) observations regarding attenuation versus mean grain size (his Fig. 3), in which attenuation peaks at ~4 ϕ (63 μm). Hamilton (1972) attributed the increase in attenuation with decreasing grain size over sands to the consequent increase in grain surface area in contact, leading to increase in loss due to internal friction. At smaller grain sizes, moving into clays, Hamilton (1972) hypothesized that an increase in cohesion with decreasing grain size acts to reduce attenuation.

Unfortunately, our comparison of overall mean grain size to attenuation does not yield any clear relationship between the two parameters, perhaps due to the fact that the sediments we sampled are commonly poorly sorted. Hence, it is difficult to make a direct comparison of our results regarding the dependence of fine % on attenuation to Hamilton's observations, although it appears likely they are related. However, we can compare our velocity versus attenuation plot (Fig. 9b) to Hamilton's (1972) published results. Although Hamilton (1972) did not directly compare these two parameters, we

Table 2
Estimation of compressional velocity (V_p) versus attenuation at 65 kHz, α_{65}, based on Hamilton's tabulations and his fig. 3 (Hamilton, 1972)

ϕ bin	$\langle V_p \rangle$ (m/s)	α_{65} (dB/m)
0.5–1.5	1777	26
1.5–2.5	1686	29
2.5–3.5	1675	37
3.5–4.5	1616	46
4.5–5.5	1552	29
5.5–6.5	1480	10

can convert his mean grain size values to velocities by averaging the tabulated velocity values within grain size bins. The bin-averaged velocities can then be associated with the attenuation value corresponding to the center grain size of the bin via Hamilton's (1972) fig. 3 (Table 2; Fig. 9b). We could, as well, use the velocity versus grain size regression equation derived by Hamilton and Bachman (1982). However, these velocity values, which were derived in the laboratory from cores, appear too high by ~100 m/s in comparison to either Hamilton's (1972) in situ velocity values or those presented in Fig. 7. Considering the scatter in our results and the approximate nature of Hamilton's curve, the comparison is reasonable. It is remarkable as well that mean sand grain size and attenuation are weakly correlated, if at all (Fig. 8b), despite the strong correlation between mean sand grain size and velocity (Fig. 7b). These results suggests that, at least for our samples, intrinsic attenuation is related more to the content of fine material than to mean grain size as Hamilton (1972) asserted.

The Biot model provides a theoretical basis for understanding the effect of pore size distribution on attenuation. Yamamoto and Turgut's (1988) modeling predicts that pore size distribution, as well as permeability, have a significant effect on attenuation. Plots of the theoretical attenuation coefficient versus grain size, generated for 14 kHz, show that increasing the standard deviation of pore size from 0 to 1.5 ϕ increases attenuation for grain sizes larger than 2 ϕ and decreases attenuation for grain sizes finer than 4 ϕ. The modeling shows that, for a given mean grain size, a change in the standard deviation of the pore size distribution from 0 to 1 ϕ may change the attenuation by as much as 10 dB. The transition between coarse and fine grain regimes is dependent on frequency: perhaps ~3–4 ϕ (~63–125 μm) at 65 kHz, as inferred from their Fig. 4. We can reasonably assume that the pore size distribution will be related to grain sorting, i.e., that a wider variance in grain sizes will result in a wider variance of pore sizes. Increasing the fine % in predominantly sandy sediments will increase grain size variance (decrease sorting) and thus, we infer, increase the variance of the pore size distribution. If true, then the positive trend we observe in attenuation versus fine % over samples with less than 22% fines (Fig. 9b) would be consistent with Yamamoto and Turgut's (1988) predictions. The evident reversal in trend at higher fine % would also be consistent with their predictions if the four samples with the highest fine % values can be considered to be within the fine-grained regime.

6.3. Spatial variability

Quantitative analyses of the spatial variability of sedimentary properties have typically focused on core-scale structural information for the purpose of investigating acoustic scattering mechanisms (e.g., Briggs et al., 1998, Jackson et al., 2002). Efforts at characterizing spatial variability on larger scales are rare (e.g., Goff et al., 2002), in large part because of the difficulties faced in obtaining samples over a large enough area and at high enough density to constrain estimation of statistical properties. One of our principal motivations for conducting this study was to ground truth the backscatter map (Fig. 2a) in order to use it as a proxy for detailed characterization of variability of the physical properties of seafloor sediments over a large area. Unfortunately, that goal was not obtainable because of the strong dependence of backscatter on coarse %, which, in turn, is not correlated with the remainder of the grain size distribution or with acoustic velocity. Nevertheless, the semi-variogram for velocity displayed in Fig. 12 provides a measure of the spatial scales of the variability of this parameter. Furthermore, the statistical model superposed on the semivariogram provides us with a basis for generating a field simulation matching the empirical statistical behavior (Fig. 13). Any number of such simulations can be generated at arbitrary resolution and coverage, providing acoustic modelers with a basis for

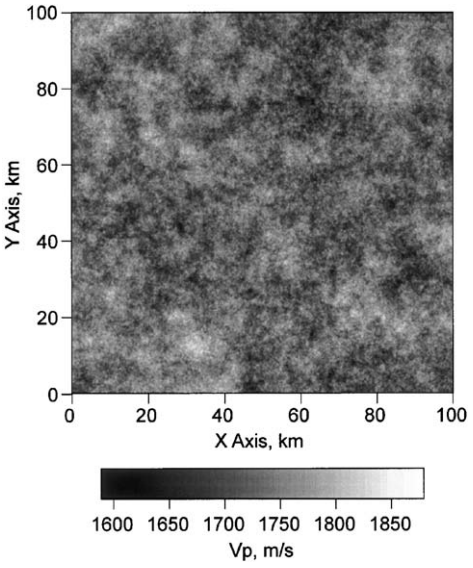

Fig. 13. Synthetic realization of the stochastic model identified in Fig. 12, generated using a Fourier method (e.g., Goff and Holliger, 1999).

conducting Monte Carlo investigations of seafloor acoustic interaction.

7. Conclusions

Our combined analysis of grain size distribution, velocity, attenuation, porosity, backscatter, and reflection coefficients demonstrate complex relationships among the physical properties, acoustic response and spatial variability of seafloor sediment on the New Jersey mid- and outer shelf. Seafloor sediments in the survey area commonly exhibit multi-modal grain size distributions, leading us to separate characterization of fine, medium (sand), and coarse contributions. The coarse % (>4 mm) represents a primary control on the backscatter, but is spatially independent of the mean sand grain size and fine %. Where the coarse % is a significant factor, which includes most of the area considered here, interpretation of the backscatter map is limited by this relationship. Where coarse % is absent, particularly in the ''high fine/low coarse'' population of sediments, then a relationship can be discerned between backscatter and velocity and between backscatter and fine %. Porosity and density may also have an influence on backscatter, but our sampling of this parameter is thus far very limited.

Mean sand grain size and fine % are partially correlated with each other and combined represent the primary control on velocity. The fine %, rather than mean grain size as a whole, appears to be the primary control on attenuation, although coarse % may increase attenuation through scattering.

The backscatter map presented in Fig. 2a is thus largely a characterization of variability in surface roughness, which locally is dominated by coarse material on the seafloor. We had hoped, based on theoretical expectations, that the backscatter map could be used as a proxy for physical parameters of importance to us: velocity, attenuation, density. However, that goal has proven unattainable as of yet. Nevertheless, we have demonstrated that where coarse material is not present in significant amounts, backscatter correlates with acoustic velocity and porosity, implying that backscatter can be used as a proxy for physical properties in those environments. In contrast to the backscatter, vertical-incidence reflection coefficients, when carefully culled of values considered unreliable and averaged to reduce variability (which also decreases resolution), did exhibit a strong correlation with in situ sediment velocity measurements. Although not nearly as cost effective as swath backscatter, high-resolution seismic data may prove to be a more reliable as a remote sensing means of sediment characterization.

Although not sufficient for deterministic mapping of seafloor velocity within the survey area, the station measurements provided important statistical information on spatial variability. Through stochastic modeling, we are able to generate synthetic realizations which conform to the statistical behavior as determined through semi-variogram analysis.

Acknowledgements

The authors wish to acknowledge the tremendous contributions to Joe Kravitz over his many years of service as ONR program manager for Marine Geology and Geophysics. Lionel Carter provided very helpful comments on an earlier draft. The Geoclutter program was among the final programs he initiated prior to his well-earned retirement. This research was funded by Office of Naval Research grants N00014-00-1-0844, N00014-01-1-0891 (JAG), N00014-00-1-0821

(LAM); N00014-00-1-0847 (SGS) and N00014-01-1-0689 (CKS). UTIG contribution 1689.

References

Andrews, D., Bennett, A., 1981. Measurements of diffusivity near the sediment–water interface with a fine-scale resistivity probe. Geochim. Cosmochim. Acta 45, 2169–2175.

Austin Jr., J.A., Fulthorpe, C.S., Mountain, G.S., Orange, D.L., Field, M.E., 1996. Continental-margin seismic stratigraphies: assessing the preservation potential of heterogeneous geological processes operating on continental shelves and slopes. Oceanography 9, 173–177.

Austin, J., Goff, J., Gulick, S., Fulthorpe, C., Nordfjord, S., Wiederspahn, M., Saustrup, S., Schock, S., Wulf, J., Gjerding, K., Mayer, L., Sommerfield, C., 2001. Assessing the "GEO" in GEOCLUTTER: new chirp sonar, sampling, and compressional wave velocity results from the New Jersey shelf. Eos Trans. AGU 82 (Abstract OS42A-0456, Fall Meet. Suppl.).

Briggs, K.B., Jackson, P.D., Holyer, R.J., Flint, R.C., Sandidge, J.C., Young, D.K., 1998. Two-dimensional variability in porosity, density and electrical resistivity of the Eckernforde Bay sediment. Cont. Shelf Res. 18, 1939–1964.

Buck, K.F., Olson, H.C., Austin Jr., J.A., 1999. Paleoenvironmental evidence for Latest Pleistocene sea level fluctuations on the New Jersey outer continental shelf: combining high-resolution sequence stratigraphy and foraminiferal analysis. Mar. Geol. 154, 287–304.

Butman, B., Noble, M., Folger, D.W., 1979. Long-term observations of bottom current and bottom sediment movement on the Mid-Atlantic continental shelf. J. Geophys. Res. 84, 1187–1205.

Chotiros, N.P., 1994. Reflection and reverberation in normal incidence echo-sounding. J. Acoust. Soc. Am. 96 (5), 2921–2929.

Chotiros, N.P., Lyons, A.P., Osler, J., Pace, N.G., 2002. Normal incidence reflection loss from a sandy sediment. J. Acoust. Soc. Am. 112 (5), 1831–1841.

Christakos, G., 1992. Random Field Models in Earth Sciences. Academic Press, New York, 474 pp.

Courtney, R.C., Mayer, L.A., 1993. Calculations of acoustic parameters by a filter correlation method. J. Acoust. Soc. Am. 93, 1145–1154.

Cressie, N., 1988. Spatial prediction and ordinary kriging. Math. Geol. 20, 405–421.

Davies, T.A., Austin Jr., J.A., Lagoe, M.B., Milliman, J.D., 1992. Late Quaternary sedimentation off New Jersey: new results using 3-D seismic profiles and cores. Mar. Geol. 108, 323–343.

Deutsch, C.V., Journel, A.G., 1992. GSLIB Geostatistical Software Library and User's Guide. Oxford Univ. Press, New York, 340 pp.

Duncan, C.S., Goff, J.A., 2001. Relict iceberg keel marks on the New Jersey outer shelf, southern Hudson Apron. Geology 29, 411–414.

Duncan, C.S., Goff, J.A., Austin, J.A., Fulthorpe, C.S., 2000. Tracking the last sea level cycle: seafloor morphology and shallow stratigraphy of the latest Quaternary New Jersey middle continental shelf. Mar. Geol. 170, 395–421.

Ewing, J., Pichon, X.l., Ewing, M., 1963. Upper stratification of Hudson Apron region. J. Geophys. Res. 68, 6303–6316.

Frankel, A., Clayton, R.W., 1986. Finite difference simulations of seismic scattering: implications for the propagation of short-period seismic waves in the crust and models of crustal heterogeneity. J. Geophys. Res. 91, 6465–6489.

Fulthorpe, C.S., Austin Jr., J.R., 1998. Anatomy of rapid margin progradation; three-dimensional geometries of Miocene clinoforms, New Jersey margin. Am. Assoc. Pet. Geol. Bull. 82, 251–273.

Fulthorpe, C.S., Goff, J.A., Austin Jr., J.A., Gulick, S.P.S., Nordfjord, S., 2002. Late Quaternary incisions and related shallow subsurface stratigraphy on the New Jersey mid-outer shelf: preliminary results from ultra-high resolution chirp sonar images—part II. Eos Trans. AGU 83 (Abstract OS71C-0300, Fall Meet. Suppl.).

Goff, J.A., 1995. Quantitative analysis of sea-ice draft: I. Methods for stochastic modeling. J. Geophys. Res. 100, 6993–7004.

Goff, J.A., Jordan, T.H., 1988. Stochastic modeling of seafloor morphology: inversion of sea beam data for second-order statistics. J. Geophys. Res. 93, 13589–13608.

Goff, J.A., Jordan, T.H., 1989. Stochastic modeling of seafloor morphology: resolution of topographic parameters by sea beam data. IEEE J. Oceanic Eng. 14, 326–337.

Goff, J.A., Swift, D.J.P., Duncan, C.S., Mayer, L.A., Hughes-Clarke, J., 1999. High resolution swath sonar investigation of sand ridge, dune and ribbon morphology in the offshore environment of the New Jersey Margin. Mar. Geol. 161, 309–339.

Goff, J.A., Olson, H.C., Duncan, C.S., 2000. Correlation of side-scan backscatter intensity with grain-size distribution of shelf sediments, New Jersey margin. Geo-Mar. Lett. 20, 43–49.

Goff, J.A., Wheatcroft, R.A., Lee, H., Drake, D.E., Swift, D.J.P., Fan, S., 2002. Spatial variability of shelf sediments in the STRATAFORM natural laboratory, Northern California. Cont. Shelf Res. 22, 1199–1223.

Hamilton, E.L., 1972. Compressional-wave attenuation in marine sediments. Geophysical 37, 620–646.

Hamilton, E.L., Bachman, R.T., 1982. Sound velocity and related properties in marine sediments. J. Acoust. Soc. Am. 72, 1891–1904.

Holliger, K., Levander, A., Goff, J.A., 1993. Stochastic modeling of the reflective lower crust: petrophysical and geological evidence from the Ivrea zone (northern Italy). J. Geophys. Res. 98, 11967–11980.

Jackson, P.D., Smith, D.T., Stanford, P.N., 1978. Resistivity–porosity–particle shape relationships for marine sands. Geophysics 43, 1250–1268.

Jackson, D.R., Winebrenner, D.P., Ishimaru, A., 1986. Application of the composite roughness model to high frequency bottom scattering. J. Acoust. Soc. Am. 79, 1410–1422.

Jackson, P.D., Briggs, K.B., Flint, R.C., Holyer, R.J., Sandidge, J.C., 2002. Two- and three-dimensional heterogeneity in carbonate sediments using resistivity imaging. Mar. Geol. 182, 55–76.

Knebel, H.J., 1979. Anomalous topography on the continental shelf around Hudson Canyon. Mar. Geol. 33, M67–M75.

Kraft, B.J., Mayer, L.A., Simpkin, P., Lavoie, P., Jabs, E., Lynskey, E., Goff, J.A., 2002. Calculation of in situ acoustic wave properties in marine sediments. In: Pace, N.G., Jensen, F.B. (Eds.), Impact of Littoral Environmental Variability on Acoustic Predictions and Sonar Performance. Kluwer, Amsterdam, pp. 123–130.

Kuo, E.Y., 1964. Wave scattering and transmission at irregular surfaces. J. Acoust. Soc. Am. 36, 2135–2142.

Makris, N.C., Ratilal, P., Lai, Y., Symonds, D.T., 2002. The Geoclutter Experiment 2001: Remote acoustic imaging of sub-bottom and seafloor morphology in continental shelf waters. J. Acoust. Soc. Am. 112, 2280.

Mayer, L.A., Hughes-Clarke, J.E., Goff, J.A., Schuur, C.L., Swift, D.J.P., 1996. Multibeam sonar bathymetry and imagery from the New Jersey continental margin: preliminary results. Eos Trans. AGU 77, F329.

Mayer, L.A., Kraft, B.J., Simpkin, P., Lavoie, P., Jabs, E., Lynskey, E., 2002. In situ determination of the variability of seafloor acoustic properties: an example from the ONR Geoclutter area. In: Pace, N.G., Jensen, F.B. (Eds.), Impact of Littoral Environmental Variability on Acoustic Predictions and Sonar Performance. Kluwer, Amsterdam, pp. 115–122.

Milliman, J.D., Jiezao, Z., Anchun, L., Ewing, J.I., 1990. Late Quaternary sedimentation on the outer and middle New Jersey continental shelf: result of two local deglaciations? J. Geol. 98, 966–976.

Murdoch, A., MacKnight, S.D., 1994. Handbook of Techniques for Aquatic Sediments Sampling. Lewis Publishers, Boca Raton, FL. 236 pp.

Nittrouer, C.A., 1999. STRATAFORM: overview of its design and synthesis of results. Mar. Geol. 154, 3–12.

Nordfjord, S., Gulick, S.P.S., Austin, J.A., Goff, J.A., Fulthorpe, C.S., 2002. Late Quaternary incisions and related shallow subsurface stratigraphy on the New Jersey mid-outer shelf: preliminary results from ultra-high resolution chirp sonar images—part I. Eos Trans. AGU 83 (Abstract OS71C-0299, Fall Meet. Suppl.).

Ogushwitz, P.R., 1985. Applicability of the Biot theory: II. Suspensions. J. Acoust. Soc. Am. 77, 441–452.

Pace, N.G., Jensen, F.B. (Eds.), 2002. Impact of Littoral Environmental Variability on Acoustic Predictions and Sonar Performance. Kluwer, Amsterdam. 632 pp.

Pettijohn, F.J., Potter, P.E., Siever, R., 1987. Sand and Sandstone, 2nd Edition. Springer-Verlag, New York. 553 pp.

Press, W.H., Flannery, B.P., Teukolsky, S.A., Vetterling, W.T., 1986. Numerical Recipes. Cambridge Univ. Press, New York. 818 pp.

Rine, J.M., Tillman, R.W., Culver, S.J., Swift, D.J.P., 1991. Generation of late Holocene ridges on the middle continental shelf of New Jersey, USA—evidence for formation in a mid-shelf setting based on comparison with a nearshore ridge. Spec. Publ. Int. Assoc. Sedimentol. 14, 395–423.

Snedden, J.W., Tillman, R.W., Kreisa Jr., R.D., Schweller, W.J., Culver, S.J., Winn, R.D., 1994. Stratigraphy and genesis of a modern shoreface-attached sand ridge, Peahala Ridge, New Jersey. J. Sediment. Res. B64, 560–581.

Stoll, R.D., 1977. Acoustic waves in ocean sediments. Geophysics 42, 715–725.

Stoll, R.D., Kan, T.K., 1981. Reflection of acoustic waves at a water–sediment interface. J. Acoust. Soc. Am. 70, 149–156.

Swift, D.J.P., Field, M.E., 1981. Evolution of a classic sand ridge field: Maryland sector, North American inner shelf. Sedimentology 28, 461–482.

Tatarski, V.I., 1961. Wave Propagation in a Turbulent Medium. McGraw-Hill, New York. 285 pp.

Twichell, D.C., Grimes, C.B., Jones, S.R., Able, K.W., 1985. The role of erosion by fish in shaping topography around Hudson submarine canyon. J. Sediment. Petrol. 55, 712–719.

Urick, R.J., 1983. Principles of Underwater Sound. McGraw-Hill, New York. 423 pp.

von Kármán, T., 1948. Progress in the statistical theory of turbulence. J. Mar. Res. 7, 252–264.

Williams, K.L., Jackson, D.R., Thorsus, E.I., Tang, D., Schock, S.G., 2002. Comparison of sound speed and attenuation measured in a sandy sediment to predictions based on the Biot theory of porous media. IEEE J. Oceanic Eng. 27, 413–428.

Wu, R.-S., Aki, K., 1985. The fractal nature of the inhomogeneities in the lithosphere evidenced from seismic wave scattering. Pure Appl. Geophys. 123, 805–818.

Yamamoto, T., 1983. Acoustic propagation in the ocean with a poro-elastic bottom. J. Acoust. Soc. Am. 73, 1587–1596.

Yamamoto, T., Turgut, A., 1988. Acoustic wave propagation through porous media with arbitrary pore size distributions. J. Acoust. Soc. Am. 83, 1744–1751.